

Network Formation and Dynamics Among Multi-LLMs

MARIOS PAPACHRISTOU, Cornell University, USA

YUAN YUAN, University of California, Davis, USA

Social networks fundamentally shape human opinions, behaviors, and the dissemination of information. As large language models (LLMs) like GPT, Claude, and Llama increasingly integrate into social and professional settings, understanding their behavior in the context of social interactions and network formation becomes essential. This study develops a framework to systematically examine whether the network formation behaviors of multiple LLMs approximate certain aspects of human network dynamics. By simulating interactions among LLM agents across various model families, we observe that these models consistently exhibit key patterns associated with social network principles—including preferential attachment, triadic closure, homophily, community structure, and the small-world phenomenon—when forming networks. Moreover, LLMs adapt their network formation strategies based on each network's characteristics, reflecting the context-dependent nature of human behavior: in Facebook networks, they prioritize triadic closure and homophily, mirroring close-knit friendships; in phone networks, homophily and preferential attachment dominate, capturing personal and professional connections, while in employment networks, LLMs favor heterophily and high-degree connections, aligning with career advancement dynamics. These results open new avenues for using LLMs in network science research, with potential applications in agent-based modeling and synthetic network generation.

Additional Key Words and Phrases: large language models, networks, network formation, link prediction, multi-agent systems

INTRODUCTION

Recent progress in large language models (LLMs), such as GPT [37], Claude [2], and Llama [47], has shown promising developments in AI techniques and their integration into real-life applications. It is thus crucial to comprehend AI actions to ensure they align with human expectations, mitigate potential risks, and maximize their benefits. Misaligned AI actions may lead to unintended consequences, such as biased decision-making, fairness issues, and the miscoordinative or non-cooperative behavior [44]. Recently, researchers have started to apply social science methodologies, such as methods analogous to laboratory experiments [1, 21, 30, 50], agent-based modeling [15, 16, 18, 20, 42, 43], and qualitative methods [11], to study LLMs. These methods not only reveal the capabilities and interpretability of LLMs but also suggest their potential for applications in social science [10, 21, 27, 41].

In human societies, social networks play a crucial role in shaping individual behaviors, preferences, and connections, as well as influencing the diffusion of information and norms across communities [3, 4, 17, 45, 54]. LLMs have shown great potential in social contexts, notably as intelligent personal assistants that facilitate social and prosocial interactions (see, e.g., [12, 40, 50]). However, less is known about how LLMs' behaviors and preferences align with human network formation principles [22, 41, 55]. This is particularly crucial, as it sheds light on the potential of these models to shape and be shaped by the networks of human relationships, which is a fundamental aspect of social systems.

Our study thus explores LLMs' behaviors and preferences in the context of network formation with both synthetic and real-world social networks. By analyzing interactions between multiple LLMs (or multi-LLMs), we aim to understand the implications of LLMs representing humans in social and professional settings. Specifically, we examine micro-level social network properties including preferential attachment [5], triadic closure [19], and homophily [32], as well as macro-level properties including community structure [36], and the small-world phenomenon [25, 52].

In synthetic network simulations, LLMs displayed preferential attachment, homophily, and triadic closure, resulting in the formation of community structures and small-world dynamics. More notably, in real-world social network simulations, we find that LLMs prioritized triadic closure and homophily over preferential attachment when forming new links, indicating a strong preference for connecting with similar nodes or shared acquaintances. Additionally, in a telecommunication network, LLMs tended to prioritize homophily and preferential attachment over triadic closure, and in a company network, the agents who corresponded to employees formed links frequently with managers, which showcases behavior that is consistent with human social mobility principles.

Generally, LLMs not only exhibit fundamental social network formation principles in synthetic simulations but also adapt their strategies based on the context of real-world networks, mirroring human social behaviors specific to each setting.

As LLM technology continues to evolve, our study serves as an early exploration of their potential in social network studies, with several significant implications for future studies. First, our study demonstrates the potential of LLMs for agent-based modeling. By simulating decision-making processes that approximate human-like behavior across various network settings, LLMs can provide valuable insights into the emergence of social phenomena. Although these models are still in early stages of development, they offer an intriguing framework for studying and designing systems that can mimic key aspects of real-world dynamics. This opens up possibilities for applying LLMs to explore and understand complex behaviors in social, professional, and collaborative environments. Second, our work highlights the potential of LLMs for synthetic dataset generation, a critical area in network science. Although the accuracy of LLM-based predictions is not yet perfect like all other link prediction models, this approach is particularly valuable in scenarios where privacy concerns limit access to real-world data. By simulating realistic datasets that capture important network properties, LLMs can facilitate research and experimentation without compromising sensitive information.

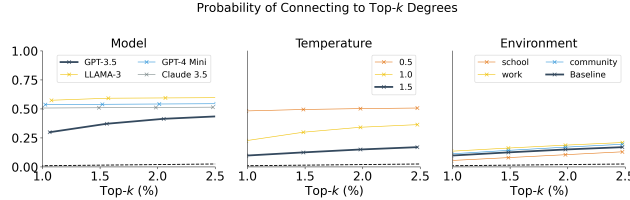
RESULTS

In this study, we investigated whether LLMs exhibit fundamental principles of network formation observed in human social networks. By simulating multiple LLM agents acting independently within separate conversational threads, we examined their behaviors in decision-making scenarios involving network connections. We focused on three micro-level network principles – preferential attachment, triadic closure, and homophily – and two macro-level phenomena—community structure and the small-world effect. To assess the robustness of our findings, we varied the temperature settings of different LLM models, including GPT-3.5-turbo, GPT-4o Mini, Llama 3 (70b-instruct), and Claude 3.5 Sonnet. We also experimented with different environmental prompts (e.g., friendship, collaboration, community) to test prompt sensitivity. Additionally, we employed an interview-like method to probe the LLMs' decision-making rationale and conducted experiments using Chain-of-Thought (CoT) reasoning [53] (the experiments are deferred to Appendix C). Finally, we extended our analysis to real-world networks, including a social media friendship network, a telecommunication network, and a company collaboration network, to compare the network formation preferences between LLMs and humans.

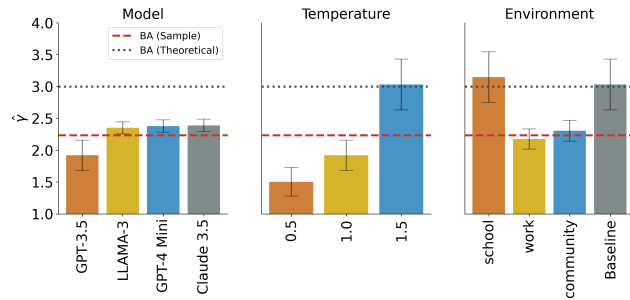
More information about the experimental procedure can be found in the *Methods and Materials* section of this paper.

Micro-Level Properties

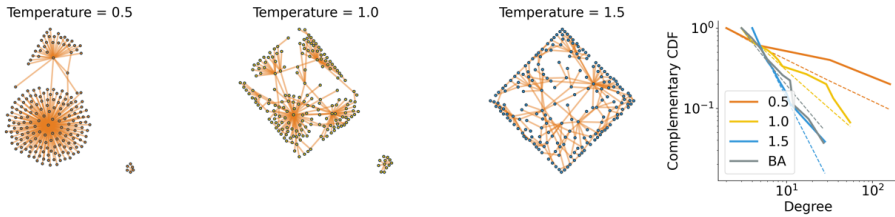
Principle 1: Preferential Attachment. Preferential attachment is a fundamental concept in network science, illustrating how nodes in a network gain connections over time, leading to a scale-free degree distribution characterized by a few highly connected nodes [5, 6].



(a) Probability of connecting to top- k nodes for different models, temperatures, and environments



(b) Power law fits (\hat{y}) and standard errors for different models, temperatures, and environments



(c) Network instances generated by GPT-3.5 agents

Fig. 1. Results for Principle 1 (preferential attachment) The multi-LLM setup was given neighborhood information $\{N_{j,t} : j \in V_t\}$. **Top:** Probability of connecting to top- k -degree nodes for varying model (temperature is fixed to 1.0 and environment to baseline), temperature (model fixed to GPT-3.5 and environment to baseline) and environment (model fixed to GPT-3.5 and environment temperature to 1.5) for networks generated according to Principle 1 with $n = 200$ nodes. **Middle:** Power Law exponents and standard errors for varying model, temperature, and environment. **Bottom:** Simulated networks. Power-law degree distributions are evident ($P > 0.5$, K-S test), with the networks at a temperature of 1.5 closely resembling the Barabási-Albert model ($P > 0.1$, K-S test) for GPT-3.5 agents.

To test if LLM agents exhibit preferential attachment, we simulated network growth by sequentially adding nodes to an initially empty network. Each new node was prompted with information about existing nodes, and the person to connect with was decided. We generated networks with $n = 200$ nodes to observe meaningful degree distributions¹.

¹Note that we provide the full network structure in the prompt, so models are not inherently biased toward forming links with the highest-degree nodes.

On a micro-scale, Figure 1(a) illustrates the probability of connecting to a top- k node as a function of its degree percentile (k/n). To demonstrate the tendency toward preferential attachment, we compare these probabilities to a null model assuming random connections (represented by dashed lines), where the likelihood of connecting to a top- k node is simply k/n . Our findings reveal that all models prefer connecting to higher-degree nodes. Notably, GPT-3.5 exhibits a weaker preference, while other, arguably more capable models, show an even stronger inclination toward preferential attachment. Using GPT-3.5 as an example, we examine the effect of temperature – a parameter controlling the variability of model output – on this tendency. At lower temperatures, the model makes fewer stochastic choices and, as a result, is more likely to connect to high-degree nodes. We also vary the prompt to explore the influence of “environment”-contextual settings such as school, work, or community. The results show slight variations compared to the baseline (GPT-3.5 with temperature = 1.5), yet the tendency for preferential attachment persists across environments. In all cases, the observed curves lie above the null model, underscoring the presence of preferential attachment.

Next, we investigate the degree distribution of the resulting graphs. As shown in Figure 1(c), the resulting networks display a pattern where a few nodes have many connections while most have few, indicative of a scale-free distribution, with form:

$$\pi(d) \propto d^{-\gamma}, \quad \text{where } \gamma > 1. \quad (1)$$

We estimated the exponent γ for different models and temperatures. Our analysis reveals several notable patterns in the networks generated by LLM agents under different conditions. First, models newer than GPT-3.5 exhibit a slightly larger $\hat{\gamma}$ than GPT-3.5. This implies that these models display a stronger tendency toward preferential attachment and the formation of hubs. Second, as the temperature increases the power-law exponent $\hat{\gamma}$ generally becomes larger. This indicates that higher temperatures introduce more variance in node connectivity, leading to degree distributions with heavier tails. Third, the environmental context significantly affects the value of $\hat{\gamma}$. For example, when the network is framed within a “school” environment, the exponent increases, suggesting a more uniform distribution of connections and fewer highly central nodes.

Finally, while the prompts we have utilized thus far have provided the model with the complete existing network structure, we also explore an alternative scenario: what happens if agents are supplied solely with the degree of other alternatives, without access to the network’s full structure? As detailed in Appendix B, our findings reveal that limiting agents to degree information alone also leads to notable structural differences in the networks that emerge (cf Figure S.9). Thus, degree information alone yields more restrictive structures than providing the agents with the full topological information (i.e. the neighbors).

The findings highlight the practical potential of LLMs in modeling complex networks, such as social, economic, or biological systems, by leveraging their ability to simulate preferential attachment and scale-free distributions. These models can be used to study real-world phenomena like information diffusion, hub formation, or connectivity patterns under varying conditions. Additionally, the sensitivity of network structures to parameters like temperature and context underscores the importance of prompt design in steering outcomes, making LLMs versatile tools for tailored simulations.

Principle 2: Triadic Closure. The second micro-level principle we examine is triadic closure, which posits that individuals are more likely to form connections with friends of friends, thus creating closed triads in the network. This process strengthens network structure and cohesion, grounded in the idea that two nodes are more likely to connect if they share a common neighbor [19, 33].

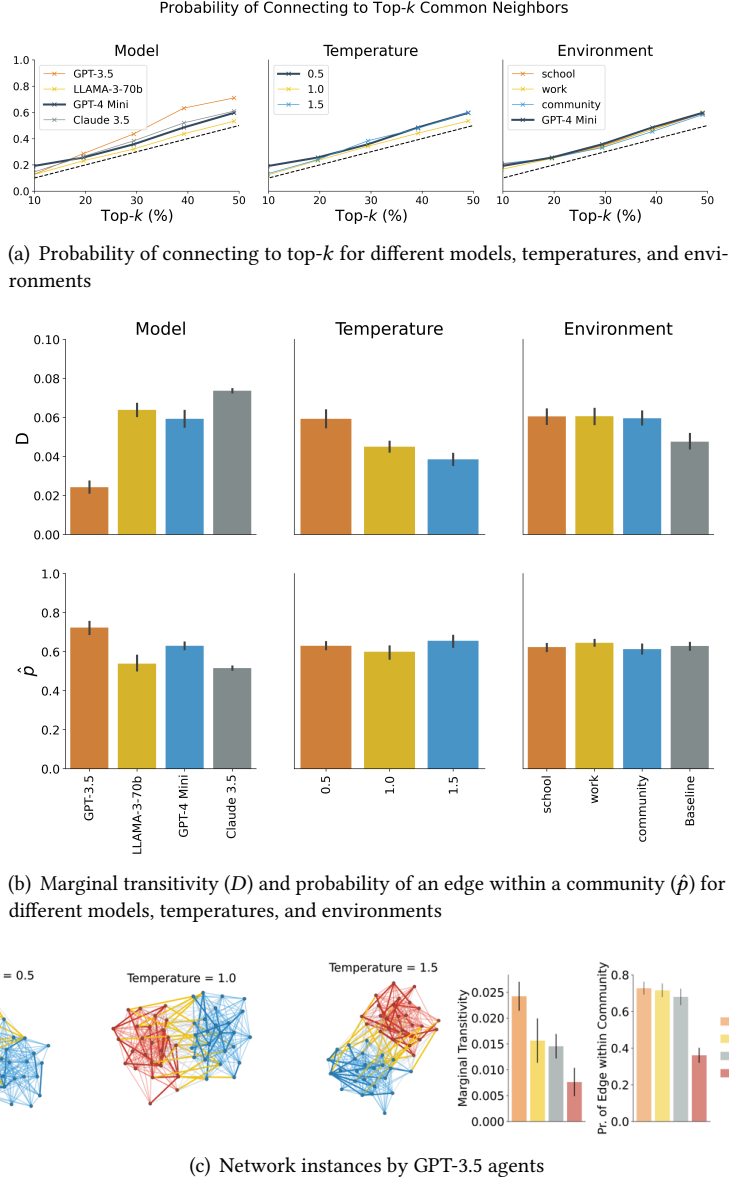


Fig. 2. Results for Principle 2 (triadic closure). **Top:** Probability of connecting to top- k nodes (in terms of common neighbors) for varying model (temperature is fixed to 1.0 and environment to baseline), temperature (model fixed to GPT-4 Mini and environment to baseline) and environment (model fixed to GPT-4 Mini and environment temperature to 0.5) for networks generated according to Principle 2 ($n = 50$, 10 simulations for each model, environment and temperature). **Middle:** Marginal transitivity (D) and probability of an edge within a community (\hat{p}) for networks generated according to Principle 2 in different models, temperatures, and environments. **Bottom:** The figure shows the resulting networks created by GPT-4 Mini, according to Principle 2 when the intersection of the neighborhoods of the query node and each alternative is provided. The node colors correspond to the groups to which each node belongs. The bold edges (red or blue) correspond to the newly created inter-cluster edges, and the orange edges correspond to the new intra-cluster edges.

To investigate triadic closure, we employ an assortative stochastic block model (SBM) [34] to create an initial network G_1 with n nodes divided into two equal-sized clusters A and B . Connections within each cluster are formed with a probability of 0.5, while inter-cluster connections occur with a probability of 0.1. This setup mirrors our assumption that nodes within the same cluster are more inclined to connect due to a higher number of shared neighbors. In subsequent time steps, we then examine each node i , considering the intersection of neighborhoods of i 's non-neighbors².

We conducted ten simulations with $n = 50$ nodes to facilitate clear visualization and ensure statistical significance³.

On a micro-scale, Figure 2(a) illustrates the probability of connecting to a top- k -percentile node as a function of the number of common neighbors. The dashed lines represent the results of null models, where connections are chosen randomly; which corresponds to the probability of connecting to a top- k percentile node in terms of the common neighbors being k/n . Our findings reveal that, across all models, there is a consistently higher probability of forming links with nodes that share more common neighbors. Unlike the behavior observed in preferential attachment, temperature does not appear to severely impact this probability. This tendency to form links with nodes that have more common neighbors is consistent across various contexts, including school, work, and community environments. These results suggest that the triadic closure tendency is a robust phenomenon, persisting across different model families, configurations, and environments.

Then, for evaluating triadic closure on the network (macroscopic) level, we utilize two metrics: *marginal transitivity* and *probability of edge formation within the same community*. Marginal transitivity (D) represents the change in the ratio of closed triangles to all triads, transitioning from the initial network G_T to the SBM-generated G_1 :

$$D = 3 \times \frac{\# \text{ triangles}(G_T)}{\# \text{ triads}(G_T)} - 3 \times \frac{\# \text{ triangles}(G_1)}{\# \text{ triads}(G_1)}.$$

where a large positive D indicates a strong triadic closure tendency. The probability of forming an edge within the same community (\hat{p}) is calculated by the ratio of edges in $G_T \setminus G_1$ (newly formed edges) connecting nodes within the same cluster:

$$\hat{p} = \frac{|\{(i, j) \in E(G_T) \setminus E(G_1) : y_i = y_j\}|}{|E(G_T) \setminus E(G_1)|},$$

where $y_i, y_j \in A, B$ denote the community memberships of nodes i and j , respectively. A value of \hat{p} exceeding 0.5 suggests a triadic closure tendency. As we investigate under SBM, same community membership indicates more open triads being closed.

Marginal transitivity (D), presented in Figure 2(b), demonstrates a statistically significant increase across all models, temperatures, and environments, underscoring the robust nature of triadic closure. Similarly, the probability of within-community edge formation (\hat{p}), shown in Figure 2(b), consistently exceeds 0.5, reaffirming the tendency of nodes to form new connections within their respective clusters.

In Figure 2(c), sample networks from GPT-3.5 are displayed, with the upper panel showing networks where the entire structure is provided and the lower panel showing those with only common neighbor numbers provided. Nodes are color-coded to indicate their cluster memberships in the SBM, with red and blue edges within clusters and orange edges between clusters. Newly formed edges are highlighted with thicker lines.

In summary, these findings show that most LLMs exhibit a consistent tendency for triadic closure across various configurations, temperatures, and environments. This behavior mirrors

²Similar outcomes arise when providing neighbors instead of common neighbors.

³Choosing $n = 50$ instead of a larger number like $n = 200$ aids in visualization and maintains statistical significance.

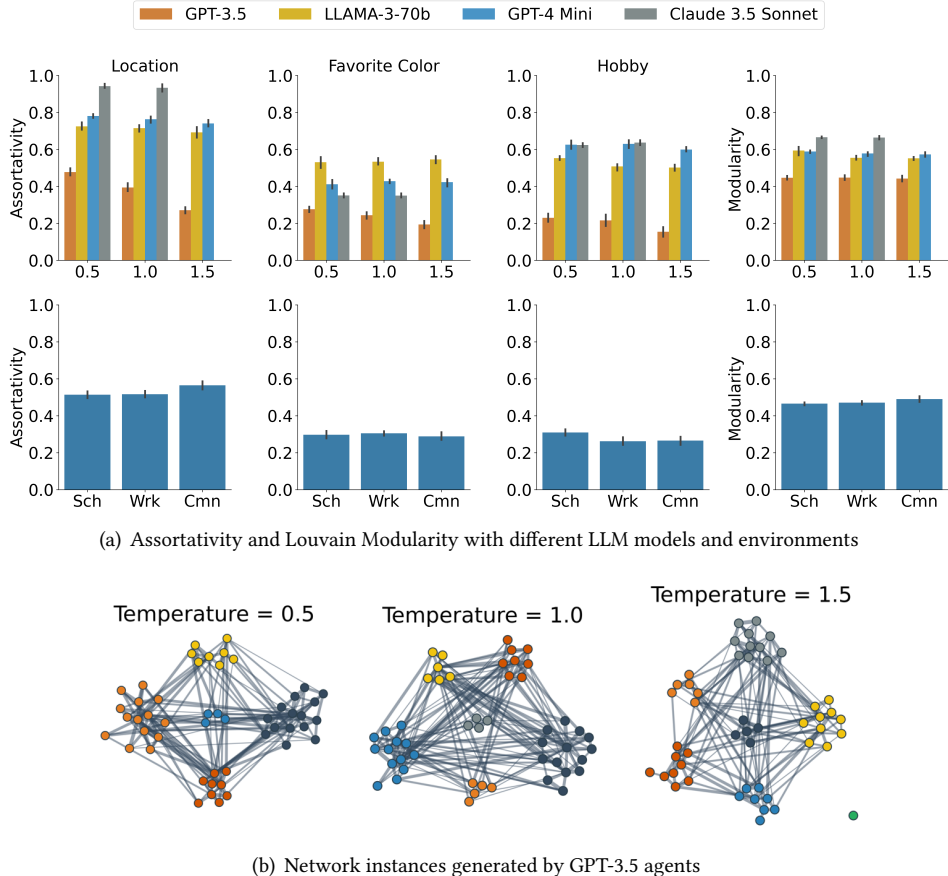


Fig. 3. Results for Principle 3 (Homophily) and Principle 4 (Community structure due to homophily). **Top:** Assortativities and Louvain modularity according to Principle 3 ($n = 50$, 5 simulations for each row) in different environments (school, work, community) using different models. The statistical significance is $P < 0.001$ for all t-tests (comparing with 0). **Bottom:** Network instances and community structure.

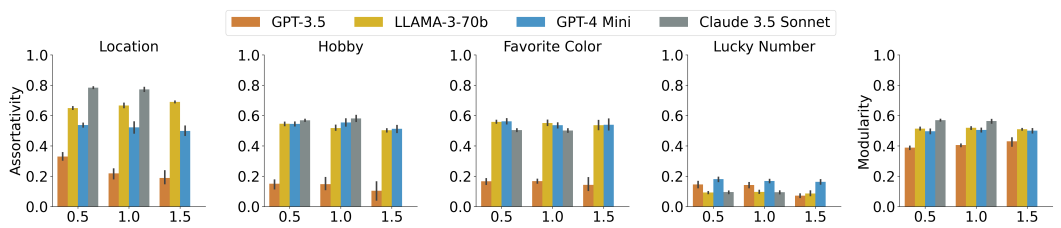


Fig. 4. Effect of distractor features (favorite color and lucky number) on homophily.

human network dynamics, highlighting the models' ability to simulate realistic social and structural networks and reinforcing their alignment with social principles observed in real-world communities.

Principle 3: Homophily. Homophily reflects the tendency for nodes with similar characteristics or attributes to form connections and associate with each other. This phenomenon is based on the principle that individuals in a network are more likely to connect with others who share similar traits, interests, or demographics [32].

To test whether LLM agents exhibit homophily, we perform the following experiment: We generate nodes with randomly generated attributes regarding a hobby (randomly chosen among three hobbies), a favorite color (randomly chosen among three colors), and a location within the US (randomly chosen among three US locations) and provide the attributes of the other nodes and the node’s own attributes, and each node is tasked to form up to $\delta = 5$ links with others. For each node i , we provide it with the features x_j of all non-neighbors j of i . The seed network is taken to be the empty graph. We run ten simulations for networks with $n = 50$ nodes and $\delta = 5$.

To evaluate homophily, we calculate the attribute assortativity coefficient for each of the features. For each property P which takes K distinct values P_1, \dots, P_K (indexed by k or l), its *assortativity coefficient* R is defined as

$$R = \frac{\sum_{k=1}^K M_{kk} - \sum_{k=1}^K a_k b_k}{1 - \sum_{k=1}^K a_k b_k}.$$

Here M represents the mixing matrix. Its elements M_{kl} reflect the proportion of edges connecting two nodes with values P_k and P_l , respectively. We define $a_k = \sum_{l=1}^K M_{kl}$ and $b_k = \sum_{l=1}^K M_{lk}$. Assortativity ranges from -1 to $+1$. A positive assortativity indicates nodes preferentially connect to similar ones, forming a homophilous network. Conversely, a negative assortativity suggests connections primarily occur between dissimilar nodes, indicating heterophily.

From Figure 3(a), we observe that different attributes exhibit varying levels of assortativity. First, homophily is present across all LLMs—regardless of the specific model or configuration (e.g., temperature settings), all show positive assortativity for all four attributes. This aligns with human societies, where homophily is a primary driver of network formation [32]⁴.

Moreover, to test the effect of the features on homophily as indicated by the assortativity coefficient for each attribute, we introduce a *distractor feature*, which corresponds to a lucky number that is randomly chosen between 0 and 9. We repeat the simulations for all models and measure the effect of each feature on Figure 4. We show that lucky numbers consistently show lower assortativity coefficients, indicating they are less considered when forming homophilous connections. This is consistent with our prior expectation that humans typically do not prioritize shared lucky numbers when establishing relationships.

Surprisingly, even though the lucky number does not seem to impact homophily much, the favorite color exhibits a similar level of homophily as hobbies. One might expect that hobbies, being substantive interests, would have a stronger influence on social connections than favorite colors, which are more arbitrary preferences. However, this finding aligns with the social identity theory and the minimal group paradigm [46]. According to this paradigm, even minimal and arbitrary group distinctions – such as a preference for certain colors – can lead to in-group favoritism and influence social connections. This suggests that LLM agents, akin to humans, may form connections based on even trivial shared attributes, reflecting inherent tendencies toward group formation based on minimal commonalities.

All in all, LLMs can capture and reproduce subtle human social behaviors, not just linguistic patterns. This underscores their potential as powerful tools for social simulation. However, these

⁴As an additional robustness check, we also tested mutual agreement connections. In that setting, after a node j is chosen by node i , j has to confirm the creation of the link from itself to i ($j \rightarrow i$). We ran several experiments with different models and temperatures and we found the results not to be affected, namely, the proposed connections were always bilateral.

findings may also raise important considerations regarding bias, fairness, and the ethical design of AI systems (cf. Discussion Section).

Macro-Level Principles

Principle 4: Community Structure. The community structure of networks refers to the organization of nodes or individuals within a network into distinct and densely interconnected groups or clusters [7, 14, 35, 36]. Identifying community structures is crucial for understanding the overall dynamics of a network, as it reveals patterns of relationships and interactions that might not be apparent at the global level.⁵

Both triadic closure and homophily contribute to the formation of community structures. By examining how these two factors contribute to network formation, we aim to gain insights into the underlying mechanisms driving community dynamics in LLM-generated networks. We employ the simulation results presented in the synthetic networks to determine whether community structure in networks generated by LLMs emerges from triadic closure or homophily.

First, we consider the networks generated in Figure 2. We examine how LLM agents' choices strengthen the network's community structure. Specifically, we leverage the fact that the SBM graph has a preexisting community structure and measure how the newly formed links reinforce such a structure. Visual inspection shows that the newly added links, represented by the bold edges, happen mostly within each cluster, reinforcing the community structure. This is further quantitatively verified by the fraction \hat{p} newly created inter-community edges. We find that \hat{p} is significantly higher than 0.5 ($P < 0.001$, t-test comparing with 0.5). This indicates that most edges are within the same community, strengthening the community structure.

Next, we investigate the community structure resulting from homophily using modularity maximization [7] (Figure 3). Modularity quantifies the discrepancy between the actual number of edges within communities and the expected number in a random network with identical node count and degree distribution, following the Chung-Lu model [13]. This model presumes that nodes maintain their weighted degree, with edges randomly distributed. The weighted modularity Q [14] for a graph with edge weights w_{ij} and C communities is defined as

$$Q = \sum_{c=1}^C \left[\frac{L_c}{W} - r \left(\frac{k_c}{2W} \right)^2 \right].$$

Here W represents the total edge weights, L_c the intra-community link weights for community c , k_c the total weighted degree within community c , and r the resolution parameter, set to 1 for our analysis. High modularity values (e.g., greater than 0.5) indicate significant community structuring, diverging from the random model.⁶

For the network's weights, we use the number of common attributes shared between each pair of nodes: $w_{ij} = \left| \left\{ k : x_i^{(k)} = x_j^{(k)} \right\} \right|$ for each link (i, j) in the final network. Here, $x_i^{(k)}$ and $x_j^{(k)}$ correspond to the k -th features of x_i and x_j , respectively.

In Figure 3(b), various colors represent the communities identified by the Louvain algorithm at different temperatures for GPT-3.5. Notably, communities appear more distinct at lower temperatures, likely due to reduced randomness in decision-making at these temperatures.

⁵As an example, we present only the results from GPT-3.5 for Principle 4 (Community Structure) and Principle 5 (Small-World).

⁶Given the NP-Hard nature of maximizing Q , we employ the Louvain algorithm [7] to approximate the highest possible modularity.

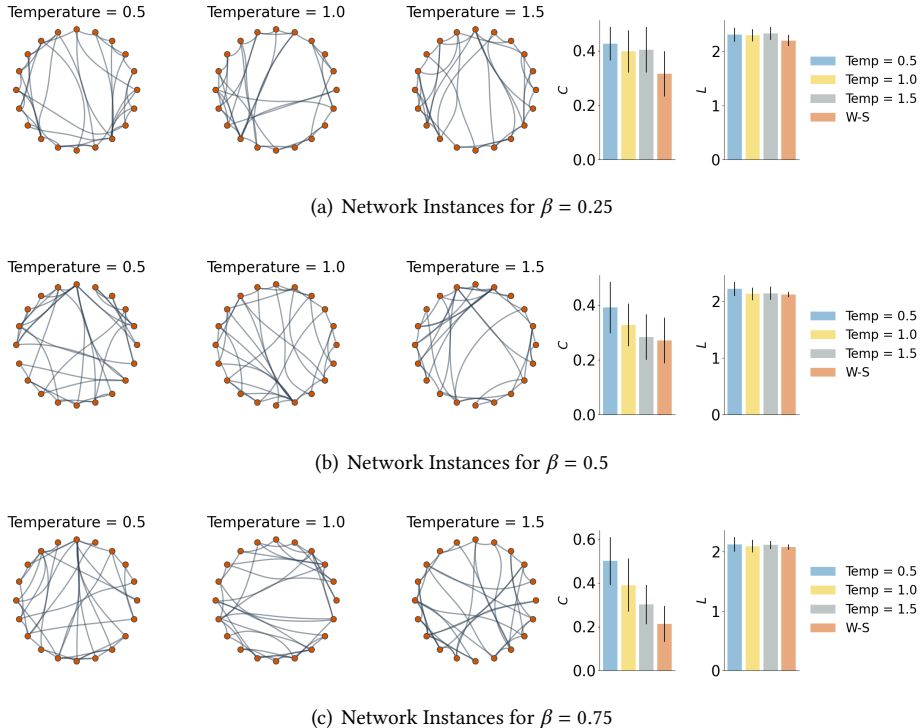


Fig. 5. Simulation results for Principle 5 (small world). Network instances for the networks created according to Principle 5 using the altered Watts-Strogatz Model for node count $n = 50$, average degree $k = 5$, rewriting probability $\beta \in \{0.25, 0.5, 0.75\}$, together with plots of the **average clustering coefficient** C and the **average shortest path length** L . The comparison is made with respect to a Watts-Strogatz graph with $n = 50, k = 5, \beta \in \{0.25, 0.5, 0.75\}$. The error bars correspond to 95% confidence intervals.

Figure 3(a) presents the distribution of Louvain modularity values across simulations across different LLM models and different environments, indicating consistent community structure with positive modularity at all temperatures, confirmed by a t-test against a modularity of $Q = 0$ for a random graph ($P < 0.001$).

Our results demonstrate that community structures manifest in networks generated by LLMs, driven by both triadic closure and homophily.

Principle 5: Small-World. The small-world phenomenon is characterized by networks where nodes are interconnected in tight clusters, yet the average distance between any two nodes remains relatively short, typically scaling logarithmically with the network size [25, 52]. This balance between high clustering and short path lengths characterizes small-world networks.

A small-world network is defined by its *average shortest path length* L , which grows logarithmically with the size of the network n ,⁷ expressed as

$$L \sim \log(n).$$

⁷As per the definition in [23].

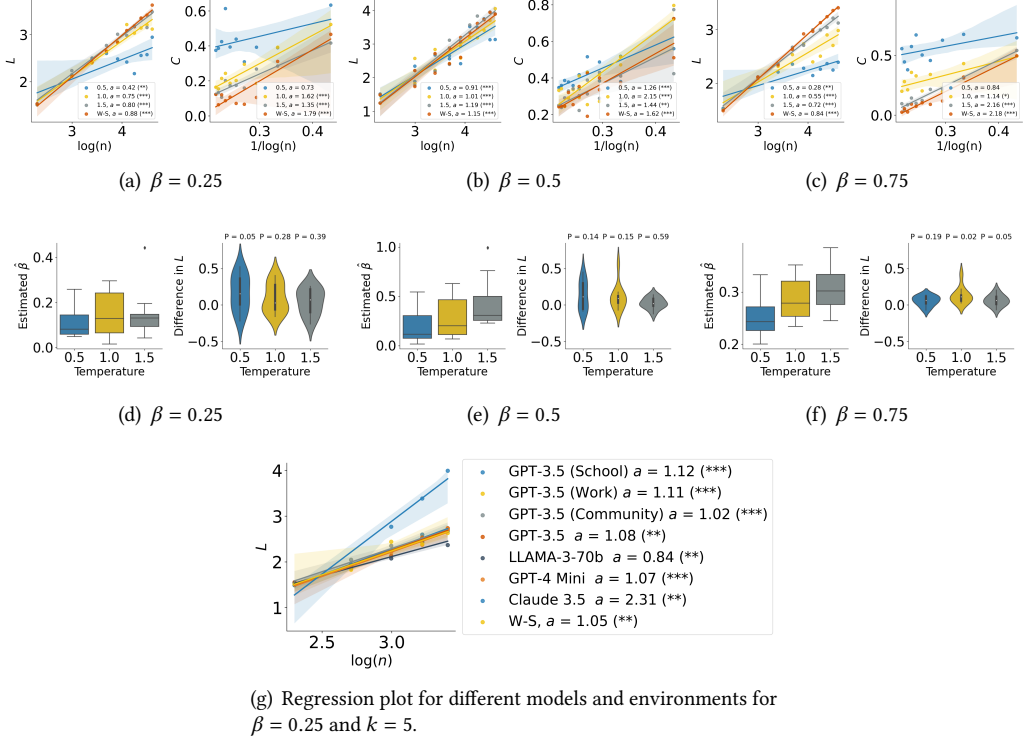


Fig. 6. Fitted results for Principle 5 (small world). **Top (a-c):** Regression plots relating **average shortest path length (L)** and **average clustering coefficient (C)** with n for $\beta \in \{0.25, 0.5, 0.75\}$ and $k = 5$ for GPT-3.5. The value a in legends represents the effect size (slope of the regression lines). **Middle (d-f):** Estimated values $\hat{\beta}$ of $\beta \in \{0.25, 0.5, 0.75\}$ for LLM-generated networks based on matching the average clustering coefficient and difference in the average shortest path between LLM-generated networks and Watts-Strogatz with the **estimated rewiring probability $\hat{\beta}$** for GPT-3.5 agents. We report the P -values of the t-test comparing the average shortest path length of the LLM-generated networks and the average shortest path length of the Watts-Strogatz graphs with rewiring probability $\hat{\beta}$. **Bottom (g):** Regression plot for the relation $L \sim \log(n)$ for different LLM models and environments (school, work, community) for $\beta = 0.25$ and $k = 5$. The legend shows the effect size (a) and the P -value. (*: $P < 0.05$; **: $P < 0.01$, and ***: $P < 0.001$.)

Our analysis utilizes the Watts-Strogatz model [52] as a benchmark to investigate whether LLMs can generate networks exhibiting small-world characteristics. This model has a delicate balance between local clustering and short average path lengths: Nodes tend to form clusters or groups (triadic closure), exhibiting a high level of interconnectedness within these local neighborhoods, whereas at the same time, the existence of a few long-range connections ensures that the entire network is reachable with relatively few steps [24, 29, 42].

We employ a modified version of the model, where edge rewiring is informed by LLM queries, based on the current network structure. The generation process is parametrized by the number of nodes (n), average degree (k), and the rewiring probability (β). See details in *Methods and Materials*.

We generated networks of various sizes, ranging from $n = 10$ to $n = 100$, to explore the relationship between the network size (n) and two key metrics: the average shortest path length (L) and the average clustering coefficient (C). For this analysis, we considered values of β set at

0.25, 0.5, and 0.75, with a fixed $k = 5$ to serve as a consistent parameter. Visual representations and average clustering coefficients are presented in Figures 5(a) to 5(c).

However, when directly compared with the Watts-Strogatz model, the networks generated by the LLMs do not precisely replicate the characteristics of Watts-Strogatz networks for the corresponding the rewiring probabilities (β). As illustrated in right panels of Figures 5(a) to 5(c), we find weak evidence that the LLM-generated networks share the same average shortest path length as the Watts-Strogatz model for the rewiring probabilities (β) of 0.25, 0.5, and 0.75, with $P < 0.1$ from a t-test comparing the average shortest path lengths. Additionally, LLM-generated networks exhibit a larger average clustering coefficient than those of the Watts-Strogatz model for the same rewiring probabilities β , also with a significance level of $P < 0.1$ in the t-test comparisons. This discrepancy suggests the differences in the network structure and connectivity patterns between the LLM-generated networks and the classical Watts-Strogatz model.

We also provide regressions analysis by examining the correlation between the average shortest path length and average clustering coefficient versus $\log(n)$ (refer to Figure 6(a), Figure 6(b), and Figure 6(c)). We found that across all tested temperatures, the relationships were statistically significant, with most regressions yielding $P < 0.001$. This indicates that the average shortest path length increases proportionally with $\log(n)$. Similarly, for the average clustering coefficient, we demonstrated that it inversely scales with $1/\log(n)$, with the majority of regression analyses also showing $P < 0.001$. These findings align with the small-world properties of organizational networks as documented in the study by [23], suggesting that these characteristics are not only prevalent but also predictable across different network sizes.

To quantify how LLM-generated networks resemble Watts-Strogatz networks, we fit the estimated $\hat{\beta}$ values for each LLM-generated network.⁸ In Figures 6(d) to 6(f), we plot the estimated values for $\hat{\beta}$ for each value of β and each temperature. Here P -values result from a t-test comparing with the average shortest path length of Watts-Strogatz with rewiring probability $\hat{\beta}$. These results show that while the average shortest path lengths are not identical, they are sufficiently close, with the differences not being statistically significant at the 0.1 level for most temperature settings. Finally, as Figure 6(g) shows, the relation $L \sim \log(n)$ holds for different LLM models and environments.

In conclusion, our analysis demonstrates that LLM-generated networks exhibit key small-world properties, with logarithmic scaling of average shortest path lengths and inverse logarithmic scaling of average clustering coefficients. While these networks do not perfectly align with the Watts-Strogatz model, they exhibit similar structural characteristics.

Decisions on Real-World Networks with Heterogeneous Agents

We investigate the behavior of LLMs in real-world network formation contexts with four datasets in two differing real-world domains. Despite the significant advancements in social network analysis over recent years, the availability of fully complete and comprehensive network datasets remains exceptionally rare [54]. We employ three datasets from the *Facebook100* collection [49] and the telecommunication (*Andorra*) and the employment (*MobileD*) datasets from [54]. The Facebook100 data correspond to “friendship” networks from one hundred American colleges and universities, captured at a specific moment from Facebook’s online social network. The Andorra dataset contains nationwide call records in Andorra from July 2015 to June 2016, where calls correspond to mutual calls between Andorran residents containing information about the caller’s and the callee’s location, phone type, and usage. Finally, the MobileD dataset corresponds to a company network where

⁸We conducted a binary search to identify the $\hat{\beta}$ values for which the Watts-Strogatz networks’ average clustering coefficients match those of the LLM-generated networks.

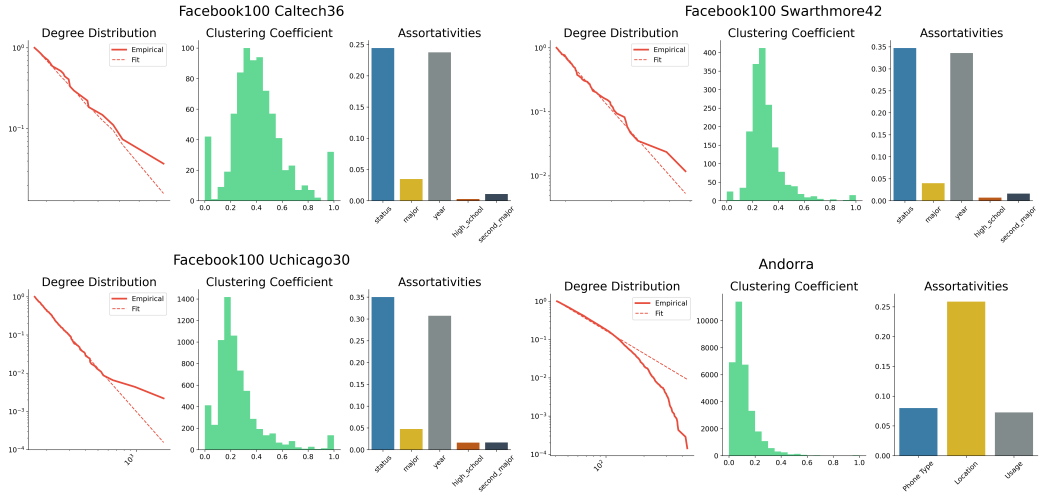


Fig. 7. Distributions of real-world datasets analyzed in our study, including degree, clustering coefficients, and the assortativities of the attributes included in the datasets.

relations correspond to call or text communication, and each employee is either a manager or a subordinate.

For all network datasets, the agents have *heterogeneous* profiles (i.e., profiles with different features) whose statistics (degree distribution, clustering coefficient distribution, assortativity) we report in Figure 7.

To infer the models' tendencies, we employ a discrete choice modeling framework [31, 38]. Specifically, we model the network formation process as a discrete choice process, wherein nodes are sequentially prompted to form connections from a set of available alternatives (see *Methods and Materials*).

Number of Samples and Alternatives. For the three datasets from Facebook100 are Caltech36 ($n = 769$) Swarthmore42 ($n = 1,659$), and UChicago30 ($n = 6,591$), we set the number of alternatives to be $A = 15$ and randomly sampled from the existing network. For the UChicago30 dataset, we consider a randomly sampled subset of $N = 2,000$ nodes because of the limited context window of the LLM models. For Andorra ($n = 32,812$) and MobileD ($n = 1,982$), we set the number of alternatives to $A = 5$ and consider a randomly sampled subset of $N = 1,000$ nodes.

Regression Coefficients. We regress network formation decisions on standardized scores reflecting the three micro-level principles. We present the regression results in Table 1.⁹ First, we observe a dominant effect of homophily across all datasets and models. The coefficients for homophily ($\hat{\theta}_H$) are consistently the largest and highly significant ($P < 0.05$) in almost all cases. For instance, in the Caltech36 dataset, the homophily coefficients for GPT-3.5, GPT-4, and Llama 3 70b Instruct are 0.65, 1.95, and 2.43, respectively ($P < 0.001$). The emphasis on homophily suggests that LLMs, much like humans, prioritize forming connections based on shared characteristics.

Second, we find that preferential attachment plays a secondary role in the network formation decisions of LLMs. While the coefficients for preferential attachment ($\hat{\theta}_{PA}$) are generally positive and statistically significant across most models and datasets, they are notably smaller than those

⁹More detailed results can be found in Table S.2 in Appendix A.

Model	Preferential Attachment ($\hat{\theta}_{PA}$)	Homophily ($\hat{\theta}_H$)	Triadic Closure ($\hat{\theta}_{TC}$)	Log Likelihood	AIC
Caltech36 ($n = 769$ nodes, $m = 33,312$ edges, $N = 769$ samples, $A = 15$ alternatives each)					
GPT-3.5	0.20*** (0.002)	0.65*** (0.005)	-0.06 (0.006)	-2,088.21	4,184.41
GPT-4o Mini	0.34*** (0.006)	2.13*** (0.03)	0.44*** (0.02)	-1,201.27	2,410.55
GPT-4 (gpt-4-1106-preview)	0.41*** (0.01)	1.95*** (0.02)	0.59*** (0.01)	-1,377.47	2,762.94
Claude 3.5 Sonnet	0.46*** (0.005)	0.55*** (0.01)	0.55*** (0.007)	-1,748.19	3,504.38
Llama 3 70b Instruct	0.28*** (0.006)	2.43*** (0.02)	0.84*** (0.01)	-809.57	1,627.15
Swarthmore42 ($n = 1,659$ nodes, $m = 122,100$ edges, $N = 1,659$ samples, $A = 15$ alternatives each)					
GPT-3.5	0.19*** (0.008)	0.47*** (0.01)	0.00 (0.009)	-4,484.45	8,976.90
GPT-4o Mini	0.27*** (0.21)	2.22*** (0.78)	0.57*** (0.43)	-1,899.09	3,806.19
GPT-4 (gpt-4-1106-preview)	0.18*** (0.003)	1.62*** (0.006)	0.65*** (0.002)	-2,838.33	5,684.66
Claude 3.5 Sonnet	0.36*** (0.002)	0.75*** (0.006)	0.55*** (0.004)	-3,563.02	7,134.03
Llama 3 70b Instruct	0.39*** (0.003)	2.31*** (0.005)	0.62*** (0.004)	-1,820.26	3,648.52
UChicago30 ($n = 6,951$ nodes, $m = 416,206$ edges, $N = 2,000$ samples, $A = 15$ alternatives each)					
GPT-3.5	0.22*** (0.001)	0.48*** (0.004)	-0.02 (0.0005)	-8,157.38	16,322.77
GPT-4o Mini	0.27*** (0.005)	2.22*** (0.19)	0.57*** (0.011)	-1,899.09	3,806.19
GPT-4 (gpt-4-1106-preview)	0.23*** (0.001)	2.00*** (0.005)	0.41*** (0.002)	-3,444.33	6,896.67
Claude 3.5 Sonnet	0.43*** (0.003)	0.78*** (0.005)	0.39*** (0.002)	-6,604.77	13,217.54
Llama 3 70b Instruct	0.43*** (0.007)	2.57*** (0.014)	0.32*** (0.005)	-3,689.00	7,386.00
Andorra ($n = 32,812$ nodes, $m = 513,931$ edges, $N = 1,000$ samples, $A = 5$ alternatives each)					
GPT-3.5	0.53*** (0.001)	0.21* (0.01)	-0.24*** (0.002)	-1,712.91	3,433.83
GPT-4o Mini	0.54*** (0.004)	3.47*** (0.06)	-0.09* (0.01)	-1,002.11	2,012.22
GPT-4 (gpt-4-1106-preview)	0.21 (0.20)	3.45*** (1.16)	-0.22 (0.25)	-1271.20	2622.30
Claude 3.5 Sonnet	0.54*** (0.003)	1.94*** (0.009)	-0.15*** (0.003)	-1,541.77	3,091.55
Llama 3 70b Instruct	0.38*** (0.003)	3.92*** (0.02)	-0.04 (0.01)	-985.95	1,979.91
MobileD ($n = 1,982$ nodes, $m = 25,470$ edges, $N = 1,000$ samples, $A = 5$ alternatives each)					
GPT-3.5	1.06*** (0.003)	-0.94*** (0.009)	-0.02 (0.001)	-1,663.42	3,334.84
GPT-4o Mini	1.38*** (0.02)	-0.85*** (0.02)	0.87*** (0.01)	-880.39	1,768.78
GPT-4 (gpt-4-1106-preview)	0.42** (0.01)	-1.84*** (0.009)	0.94*** (0.003)	-1,321.01	2,650.02
Claude 3.5 Sonnet	0.71*** (0.009)	-2.44*** (0.02)	1.13*** (0.005)	-1,197.92	2,403.83
Llama 3 70b Instruct	1.04*** (0.005)	-0.36** (0.01)	0.71*** (0.002)	-1,269.42	2,546.83

Note: *: $P < 0.05$, **: $P < 0.01$, ***: $P < 0.001$

Table 1. Effect sizes for real-world networks from Facebook100 [49] and Andorra dataset [54] for several LLMs for temperature set to 0.5. An earlier version of this paper included experiments with gpt-4-1106-preview beyond gpt-4o-mini. We have also added these experiments for completeness.

for homophily. For example, in the Swarthmore42 dataset, GPT-3.5 and Llama 3 70b Instruct have preferential attachment coefficients of 0.19 and 0.39, respectively ($P < 0.001$). This suggests that while LLMs do consider the degree of potential connection nodes—favoring connections to well-connected nodes—the influence of this factor is less evident compared to homophily.

Finally, the influence of triadic closure appears to vary across different datasets and models. In most cases, the coefficients for triadic closure ($\hat{\theta}_{TC}$) are positive and significant, indicating that LLMs consider the number of mutual connections when forming new links. However, in some instances, such as with GPT-3.5 on the Andorra dataset, the triadic closure coefficient is negative (-0.24) and significant, suggesting a structure-dependent role of this principle as shown by the low clustering coefficient of the network, which is dominated by preferential attachment, as also shown in Figure 7. This variability implies that while triadic closure is a factor in LLMs’ decision-making, its impact may be influenced by the specific characteristics of the dataset or the model used.

In summary, our analysis demonstrates that while homophily, triadic closure, and preferential attachment are integral to the network formation behaviors of LLMs, homophily is the dominant factor.

DISCUSSION

Summary of Findings and Broader Impact. In this study, we conducted a comprehensive evaluation of LLMs' network formation preferences, examining both micro-level network principles—such as preferential attachment, triadic closure, and homophily—and macro-level network properties like community structure and the small-world phenomenon. Our findings indicate that networks generated by multiple LLMs exhibit these properties, particularly when the models are primed with network statistics like the number of mutual friends or the degrees of potential connections. Furthermore, using discrete choice modeling, we explored the emergence of these properties in simulations based on real-world networks. Our results reveal that the LLM agents' selections are predominantly driven by homophily, followed by triadic closure and preferential attachment.

On the one hand, our study enhances our understanding of how multiple LLMs behave in networked settings. Specifically, our findings reveal varying strengths in network formation properties among LLMs, suggesting that when these models are employed to coordinate social networks in social or work environments, they may exhibit human-like behaviors. This has important implications for applications like agent-based modeling, where realistic simulation of human behavior is crucial. Traditionally, agent-based models rely on simplified rules or heuristics to represent individual behaviors, which may not capture the complexity of human decision-making. By incorporating LLMs as agents, we can simulate more nuanced and context-aware interactions that closely resemble human social behavior, without the need to rigidly specify decision rules or heuristics.

Limitations and Boundary Conditions. On the other hand, our results suggest that we should exercise caution when leveraging LLMs in networking scenarios. The model family, configuration, and prompts can subtly affect the models' behavior, resulting in qualitatively similar but quantitatively different outcomes.

For example, newer models such as GPT-4 and Claude 3.5 exhibit stronger biases compared to prior models such as GPT-3.5. For instance, in the preferential attachment principle, newer models such as GPT-4 and Claude 3.5 have stronger biases – i.e., connect to *highest-degree-nodes* yielding star-like networks – compared to GPT-3.5 and LLama 3, which had weaker biases – i.e., connect to *high-degree-nodes*. Similar results can be found in homophily, as larger biases towards homophily, and triadic closure. Thus, even though LLMs exhibit these principles, we should be cautious of such biases when designing simulations.

Similarly, in our experiments with real-world data, we find an interesting phase transition from homophily to heterophily: In the Facebook100 data, the LLMs generally exhibited positive biases toward homophily ($\hat{\theta}_H > 0$). However, in employment networks, agents were either managers or subordinates, and we discovered that LLM agents were heterophilous in such a case ($\hat{\theta}_H < 0$), which aligns with career advancement dynamics (i.e. employees want to form links with managers because of better career prospects).

The above underscores the need for researchers to provide oversight and ensure that LLM behaviors align with human expectations when employing them in scientific research methods, such as agent-based modeling and even prototypical human subject research with LLMs.

Thus, although we find that LLMs resemble human network formation behaviors, we should consider whether these models should exhibit such behaviors when serving as assistants to humans in work and social lives. Biases like homophily, triadic closure, or preferential attachment may lead to network structures that overemphasize certain individuals or fragment information flow. Humans form networks with communities and central nodes partly due to limited social capacities; however, LLMs do not share these limitations.

Therefore, when used as social assistants, LLMs may not necessarily need to mirror human networking behaviors and could be personalized to promote more equitable and efficient information

dissemination. Our study highlights the need for more deliberate efforts to align LLM behavior in this domain.

Future Research Directions. Looking ahead, we identify three promising directions for future research: First, investigating LLM behavior in more complex interactions, such as simulated dialogues, could provide deeper insights. By examining the specific dialogues of LLMs during interactions, we can better understand their network formation preferences and how they adapt to different social dynamics. Second, we could explore how LLMs can be integrated into real-world settings, such as social media platforms. LLM-assisted bots might be employed to facilitate interactions, break echo chambers, and moderate democratic discussions (see, for example, [40]).

Finally, we can use our methods to create realistic synthetic networks. These synthetic datasets can serve as benchmarks for evaluating graph learning methods, thereby addressing the scarcity of existing graph benchmarks (cf. [39]). By adjusting parameters like temperature and environmental settings or selecting different models, we can generate diverse networks to test graph neural network performance under various conditions. Importantly, our approach allows for the generation of artificial data that resembles real-world data while adhering to privacy regulations.

METHODS AND MATERIALS

Experimental Procedure

In our study, we performed experiments to assess whether key network principles at both the micro-level (such as preferential attachment, triadic closure, and homophily) and the macro-level (including community structure and weak ties) align with classical network models. Subsequently, we utilized real-world networks to determine the factors that are most heavily weighted by LLMs.

Network Formation Process. Our experiments span a time series of T steps, with a sequence of network structures denoted as G_1, G_2, \dots, G_T with vertex sets V_1, \dots, V_T . The initial network, G_1 , is referred to as the *seed network*. At each step t , we select a *query node* i_t (which may either be a new arrival or an existing node in the graph) and assign it the task of forming new links. This is accomplished by selecting nodes from a set of alternatives A_t (meaning potential candidates for link formation) and initiating a query call $Q(A_t, i_t, \delta)$ to the LLM (as outlined in Algorithm 2) to create up to δ new links. The edge set selection process involves presenting the LLMs with personal or network features of the alternatives, denoted as $F(A_t) = \{f_a : a \in A_t\}$, which may include information such as the neighbors of the nodes, node degrees, common connections with i_t , and community memberships, formatted in JSON. We adopt a zero-shot learning approach, avoiding the provision of examples to the model to prevent bias, in line with relevant studies such as [9]. This approach allows for the exploration of the innate preferences of LLMs.

We employ multiple temperatures to account for the variability in response generation by LLM systems, which is also observed in classical statistical models of network formation [22]. Our study conducts experiments using three temperatures for all models except Claude 3.5: 0.5, 1.0, and 1.5. For Claude 3.5 the temperature range is between 0 and 1, and we run experiments with two temperatures: 0.5, and 1.0.

Moreover, the model is tasked with outputting a JSON object indicating the node chosen for link formation and the rationale behind the choice. This approach is adopted because LLMs have demonstrated proficiency in processing code-like structures, such as HTML and JSON.

Feature Representations for Prompts. Below, we give examples of the features used in the prompt presented in Algorithm 2. The features are formatted as a list of JSON objects which are provided to the prompt.

ALGORITHM 1: Example prompt regarding social network data.

```

# Task
You are located in a school. Your task is to select a set of people to be friends with.

# Profile
Your profile is given below after chevrons:
<PROFILE>
{
    "name" : "Person 0",
    "favorite subject" : "Chemistry",
    "neighbors" : ["Person 3", "Person 432", "Person 4", "Person 3", "Person 32"]
}
</PROFILE>

# Candidate Profiles
The candidate profiles to be friends with are given below after chevrons:

<PROFILES>
[
    {
        "name" : "Person 1",
        "favorite subject" : "Mathematics",
        "neighbors" : ["Person 3", "Person 4", "Person 23", "Person 65"]
    },
    {
        "name" : "Person 33",
        "favorite subject" : "History",
        "neighbors" : ["Person 342", "Person 2", "Person 12"]
    },
    ...
]

</PROFILES>

# Output
The output should be given a list of JSON objects with the following structure

[
    {
        "name" : name of the person you selected,
        "reason" : reason for selecting the person
    },
    ...
]

# Notes
- The output must be a list of JSON objects ranked in the order of preference.
- You can make at most 1 selection.

```

Principle 1: Preferential Attachment. We have the following features:

```

[
    {
        "name" : 0,
        "neighbors" : [5, 7, 1, 6]
    },
    ...
]

```

Principle 2: Triadic Closure. We have the following features:

```

[
    {

```

ALGORITHM 2: General Prompt used to implement $Q(A_t, i_t, \delta)$.

```

# Task
Your task is to select a set of people to be friends with.

# Profile
Your profile is given below after chevrons:
<PROFILE>F({ $i_t$ })</PROFILE>

# Candidate Profiles
The candidate profiles to be friends with are given below after chevrons:
<PROFILES>F( $A_t$ )</PROFILES>

# Output
The output should be given a list of JSON objects with the following structure

[
  {
    "name" : name of the person you selected,
    "reason" : reason for selecting the person
  }, ...
]

# Notes
- The output must be a list of JSON objects ranked in the order of preference.
- You can make at most  $\delta$  selections.

```

```

    "name" : 0,
    "common_neighbors" : [5, 7, 1, 6]
  },
  ...
]
```

Principle 3: Homophily. We have the following features:

```

[
  {
    "name" : 0,
    "favorite_color" : "red",
    "hobby" : "hiking",
    "location" : "Boston"
  },
  ...
]
```

Principle 5: Small-World. We have the following features:

```

[
  {
    "name" : 0,
    "neighbors" : [5, 7, 1, 6]
  },
  ...
]
```

Real-World Data. We have the following features:

```

[
  {
    "name" : 0,
    "status" : "student",
    "major" : 10,
```

```

    "second_major" : 93,
    "accommodation" : "house",
    "high_school" : 5,
    "graduation_year" : 2008
  },
  ...
]

```

We note that the initial Facebook100 dataset included gender information as a feature. We chose not to include gender as one of the features as it has been shown that language models exhibit gender bias [8, 26, 51]. An example of the prompt using real-world social network data is given at Algorithm 1.

Robustness Checks. We tried the following LLM models:

- GPT-3.5 (gpt-3.5-turbo)
- GPT-4o Mini (gpt-4o-mini)
- Llama 3 (llama-3-70b-instruct)
- Claude 3.5 Sonnet (claude-3-5-sonnet-20240620).

For each of the models except Claude 3.5 we used three temperatures: 0.5, 1.0, 1.5. For the Claude 3.5 model we used temperatures 0.5 and 1.0 (since the model does not allow temperatures above 1.0). Finally, we experimented with different environmental prompts (e.g., friendship, collaboration, community) to test prompt sensitivity.

Details for Small-World Experiments

The algorithm for the altered Watts-Strogatz model is described as follows:

- (1) Similarly to Watts-Strogatz, we first create a ring network with n nodes. After that, for each node $[n]$, we create k edges where $k/2$ edges connect to its rightmost neighbors and $k/2$ edges connect to its leftmost neighbors.
- (2) To create G_t , for each node $[n]$, we take its $k/2$ rightmost neighbors and rewire them with probability β . For each of the $k/2$ rightmost neighbors that are to be rewired, we make one query to the LLM, which indicates how the edge will be rewired. The choice is made by providing the LLM with all the network nodes and each node's neighbors (i.e., the network structure).

The model closely resembles the Watts-Strogatz model, with the primary distinction being the method of edge rewiring. Instead of randomly selecting edges for rewiring, as in the Watts-Strogatz model, we determine the rewiring of an edge by inquiring about the LLM and providing it with the current network structure.

The Discrete Choice Model in Real-World Network Experiments

For each node i_t that we consider at time t , we randomly remove one of its current friends from the real-world network. After we remove a neighbor for each of i_1, \dots, i_T , we end up with the network G_1 , which we use as a seed network for the LLM agents.

Subsequently, during the link formation process, we present each node i_t with a set of candidate nodes (denoted by A_t), comprising one of the previously removed friends and other nodes that are not their friends. We then instruct the LLM to form a link with one of the candidates, providing the attributes of the candidates and the social network structure to aid its decision-making. These choices are made sequentially.

We use the *utility* of the model for each node for each sequential decision of network formation:

$$U_{ij,t} = \theta_{PA} \log d_{j,t} + \theta_H \log w_{ij} + \theta_{TC} \log c_{ij,t} + \epsilon_{ij,t}.$$

In this equation, θ_{PA} measures the strength of preferential attachment based on the degree $d_{j,t}$ of j at step t , θ_H measures the strength of homophily based on the similarity w_{ij} (i.e. number of common attributes) between i and j , and θ_{TC} measures the strength of triadic closure, based on the number of common neighbors $c_{ij,t}$ between i and j at step t . The error term $\epsilon_{ij,t}$ is distributed as i.i.d. standard Gumbel.¹⁰ All variables are first normalized based on their range, and then the log transformation is taken.

The multinomial logit model (MNL) indicates that the probability that i links to j at step t is given by

$$p_{ij,t} = \Pr \left[\operatorname{argmax}_{r \in A_t} U_{ir,t} = j \right] = \frac{d_{j,t}^{\theta_{PA}} w_{ij}^{\theta_H} c_{ij,t}^{\theta_{TC}}}{\sum_{r \in A_t} d_{r,t}^{\theta_{PA}} w_{ir}^{\theta_H} c_{ir,t}^{\theta_{TC}}}.$$

Given a sequence of nodes $i_1, \dots, i_T \in V$ and choices (denoted by subscripted j) $j_1 \in A_1, \dots, j_T \in A_T$, the parameters can be found by maximizing the log-likelihood function. To get the standard errors of the coefficients and the corresponding P -values, we follow the process outlined in [38].

Estimating the Parameters of the Discrete Choice Model

To estimate the parameters of the discrete choice model, we optimize the following log-likelihood function

$$(\hat{\theta}_{PA}, \hat{\theta}_{TC}, \hat{\theta}_H) = \arg \max_{(\theta_{PA}, \theta_{TC}, \theta_H) \in \mathbb{R}^3} \sum_{t=1}^T \left(\theta_{PA} \log d_{j_t,t} + \theta_H \log w_{i_t j_t} + \theta_{TC} \log c_{i_t j_t, t} - \log \left(\sum_{r \in A_t} d_{r,t}^{\theta_{PA}} w_{i_t r}^{\theta_H} c_{i_t r, t}^{\theta_{TC}} \right) \right),$$

where i_1, \dots, i_T are the chooser nodes (i.e., the LLM agents who want to form a link), and j_1, \dots, j_T are the nodes which are chosen from the alternative sets A_1, \dots, A_T . The likelihood function is convex, and we optimize it with the L-BFGS-B method [28]. The standard errors of the coefficients are approximated as $\sqrt{-H^{-1}/N}$ where H is the Hessian matrix of the log-likelihood at $(\hat{\theta}_{PA}, \hat{\theta}_{TC}, \hat{\theta}_H)$ and N is the number of data points (cf. [38, 48]).

Data and Code Availability

Data and code are available on GitHub at the following link:

<https://github.com/papachristoumarios/llm-network-formation>

The real-world social network data have been taken from the sources of [49] and [54].

ACKNOWLEDGMENTS

The authors would like to thank Jon Kleinberg, Yanbang Wang, Yuanqi Du, the attendees of the Learning on Graphs NYC meetup, and the participants of Cornell AI, Policy, and Practice working group for their valuable feedback on the current version of the paper. M.P. is supported by a scholarship from the Onassis Foundation (Scholarship ID: F ZT 056-1/2023-2024).

REFERENCES

- [1] Gati V Aher, Rosa I Arriaga, and Adam Tauman Kalai. 2023. Using large language models to simulate multiple humans and replicate human subject studies. In *International Conference on Machine Learning*. PMLR, 337–371.
- [2] Anthropic. 2024. Claude: Large Language Model by Anthropic. <https://www.anthropic.com/> Accessed: 2024-09-18.
- [3] Eytan Bakshy, Itamar Rosenn, Cameron Marlow, and Lada Adamic. 2012. The role of social networks in information diffusion. In *Proceedings of the 21st international conference on World Wide Web*. 519–528.

¹⁰The standard Gumbel distribution has CDF $e^{e^{-x}}$.

- [4] Abhijit Banerjee, Arun G Chandrasekhar, Esther Duflo, and Matthew O Jackson. 2013. The diffusion of microfinance. *Science* 341, 6144 (2013), 1236498.
- [5] Albert-László Barabási and Réka Albert. 1999. Emergence of scaling in random networks. *Science* 286, 5439 (1999), 509–512.
- [6] Ginestra Bianconi and A-L Barabási. 2001. Competition and multiscaling in evolving networks. *Europhysics letters* 54, 4 (2001), 436.
- [7] Vincent D Blondel, Jean-Loup Guillaume, Renaud Lambiotte, and Etienne Lefebvre. 2008. Fast unfolding of communities in large networks. *Journal of statistical mechanics: theory and experiment* 2008, 10 (2008), P10008.
- [8] Shikha Bordia and Samuel R Bowman. 2019. Identifying and reducing gender bias in word-level language models. *arXiv preprint arXiv:1904.03035* (2019).
- [9] Philip Brookins and Jason Matthew DeBacker. 2023. Playing games with GPT: What can we learn about a large language model from canonical strategic games? *Available at SSRN* 4493398 (2023).
- [10] Yiting Chen, Tracy Xiao Liu, You Shan, and Songfa Zhong. 2023. The Emergence of Economic Rationality of GPT. *arXiv preprint arXiv:2305.12763* 120, 51 (2023), e2316205120. <https://doi.org/10.1073/pnas.2316205120> arXiv:<https://www.pnas.org/doi/pdf/10.1073/pnas.2316205120>
- [11] Robert Chew, John Bollenbacher, Michael Wenger, Jessica Speer, and Annice Kim. 2023. LLM-assisted content analysis: Using large language models to support deductive coding. *arXiv preprint arXiv:2306.14924* (2023).
- [12] Felix Chopra and Ingar Haaland. 2023. Conducting qualitative interviews with AI. *CESifo Working Paper* (2023).
- [13] Fan Chung and Linyuan Lu. 2004. The average distance in a random graph with given expected degrees. *Internet Mathematics* 1, 1 (2004), 91–113.
- [14] Aaron Clauset, Mark EJ Newman, and Christopher Moore. 2004. Finding community structure in very large networks. *Physical review E* 70, 6 (2004), 066111.
- [15] Giordano De Marzo, Luciano Pietronero, and David Garcia. 2023. Emergence of Scale-Free Networks in Social Interactions among Large Language Models. *arXiv preprint arXiv:2312.06619* (2023).
- [16] Bahare Fatemi, Jonathan Halcrow, and Bryan Perozzi. 2023. Talk like a graph: Encoding graphs for large language models. *arXiv preprint arXiv:2310.04560* (2023).
- [17] James H Fowler and Nicholas A Christakis. 2008. Dynamic spread of happiness in a large social network: longitudinal analysis over 20 years in the Framingham Heart Study. *Bmj* 337 (2008).
- [18] Chen Gao, Xiaochong Lan, Zhihong Lu, Jinzhu Mao, Jinghua Piao, Huandong Wang, Depeng Jin, and Yong Li. 2023. S3: Social-network Simulation System with Large Language Model-Empowered Agents. *arXiv preprint arXiv:2307.14984* (2023).
- [19] Mark S Granovetter. 1973. The strength of weak ties. *American journal of sociology* 78, 6 (1973), 1360–1380.
- [20] James He, Felix Wallis, and Steve Rathje. 2023. Homophily in An Artificial Social Network of Agents Powered by Large Language Models. *OSF* (2023).
- [21] John J Horton. 2023. *Large language models as simulated economic agents: What can we learn from homo silicus?* Technical Report. National Bureau of Economic Research.
- [22] Matthew O Jackson. 2008. *Social and economic networks*. Vol. 3. Princeton university press Princeton.
- [23] Abigail Z Jacobs and Duncan J Watts. 2021. A large-scale comparative study of informal social networks in firms. *Management Science* 67, 9 (2021), 5489–5509.
- [24] Eaman Jahani, Samuel P Fraiberger, Michael Bailey, and Dean Eckles. 2023. Long ties, disruptive life events, and economic prosperity. *Proceedings of the National Academy of Sciences* 120, 28 (2023), e2211062120.
- [25] Jon Kleinberg. 2000. The small-world phenomenon: An algorithmic perspective. In *Proceedings of the thirty-second annual ACM symposium on Theory of computing*. 163–170.
- [26] Hadas Kotek, Rikker Dockum, and David Sun. 2023. Gender bias and stereotypes in Large Language Models. In *Proceedings of The ACM Collective Intelligence Conference*. 12–24.
- [27] Yan Leng, Tara Sowrirajan, Yujia Zhai, and Alex Pentland. 2023. Interpretable stochastic block influence model: measuring social influence among homophilous communities. *IEEE Transactions on Knowledge and Data Engineering* (2023).
- [28] Dong C Liu and Jorge Nocedal. 1989. On the limited memory BFGS method for large scale optimization. *Mathematical programming* 45, 1 (1989), 503–528.
- [29] Ding Lyu, Yuan Yuan, Lin Wang, Xiaofan Wang, and Alex Pentland. 2022. Investigating and modeling the dynamics of long ties. *Communications Physics* 5, 1 (2022), 87.
- [30] Benjamin S Manning, Kehang Zhu, and John J Horton. 2024. Automated Social Science: A Structural Causal Model-Based Approach. *SSRN* (2024).
- [31] Daniel McFadden. 1972. Conditional logit analysis of qualitative choice behavior. *Working Paper* (1972).
- [32] Miller McPherson, Lynn Smith-Lovin, and James M Cook. 2001. Birds of a feather: Homophily in social networks. *Annual review of sociology* 27, 1 (2001), 415–444.

- [33] Mohsen Mosleh, Dean Eckles, and David Gertler Rand. 2024. *Tendencies toward triadic closure: Field-experimental evidence*. Technical Report. Center for Open Science.
- [34] Mark EJ Newman. 2003. Mixing patterns in networks. *Physical review E* 67, 2 (2003), 026126.
- [35] Mark EJ Newman. 2006. Modularity and community structure in networks. *Proceedings of the national academy of sciences* 103, 23 (2006), 8577–8582.
- [36] Mark EJ Newman and Michelle Girvan. 2004. Finding and evaluating community structure in networks. *Physical review E* 69, 2 (2004), 026113.
- [37] OpenAI. 2023. GPT-4 technical report. *arXiv* (2023), 2303–08774.
- [38] Jan Overgoor, Austin Benson, and Johan Ugander. 2019. Choosing to grow a graph: Modeling network formation as discrete choice. In *The World Wide Web Conference*. 1409–1420.
- [39] John Palowitch, Anton Tsitsulin, Brandon Mayer, and Bryan Perozzi. 2022. Graphworld: Fake graphs bring real insights for gnns. In *Proceedings of the 28th ACM SIGKDD Conference on Knowledge Discovery and Data Mining*. 3691–3701.
- [40] Marios Papachristou, Longqi Yang, and Chin-Chia Hsu. 2023. Leveraging Large Language Models for Collective Decision-Making. *arXiv preprint arXiv:2311.04928* (2023).
- [41] Joon Sung Park, Joseph C O'Brien, Carrie J Cai, Meredith Ringel Morris, Percy Liang, and Michael S Bernstein. 2023. Generative agents: Interactive simulacra of human behavior. *arXiv preprint arXiv:2304.03442* (2023), 1–22.
- [42] Patrick S Park, Joshua E Blumenstock, and Michael W Macy. 2018. The strength of long-range ties in population-scale social networks. *Science* 362, 6421 (2018), 1410–1413.
- [43] Bryan Perozzi, Bahare Fatemi, Dustin Zelle, Anton Tsitsulin, Mehran Kazemi, Rami Al-Rfou, and Jonathan Halcrow. 2024. Let Your Graph Do the Talking: Encoding Structured Data for LLMs. *arXiv preprint arXiv:2402.05862* (2024).
- [44] Iyad Rahwan, Manuel Cebrian, Nick Obradovich, Josh Bongard, Jean-François Bonnefon, Cynthia Breazeal, Jacob W Crandall, Nicholas A Christakis, Iain D Couzin, Matthew O Jackson, et al. 2019. Machine behaviour. *Nature* 568, 7753 (2019), 477–486.
- [45] E. M. Rogers. 2003. *Diffusion of Innovations* (5th ed.). Simon and Schuster.
- [46] Henri Tajfel, Michael G Billig, Robert P Bundy, and Claude Flament. 1971. Social categorization and intergroup behaviour. *European journal of social psychology* 1, 2 (1971), 149–178.
- [47] Hugo Touvron, Louis Martin, Kevin Stone, Peter Albert, Amjad Almahairi, Yasmine Babaei, Nikolay Bashlykov, Soumya Batra, Prajjwal Bhargava, Shruti Bhosale, Dan Bikel, Lukas Blecher, Cristian Canton Ferrer, Moya Chen, Guillem Cucurull, David Esiobu, Jude Fernandes, Jeremy Fu, Wenyin Fu, Brian Fuller, Cynthia Gao, Vedanuj Goswami, Naman Goyal, Anthony Hartshorn, Saghaf Hosseini, Rui Hou, Hakan Inan, Marcin Kardas, Viktor Kerkez, Madian Khabsa, Isabel Kloumann, Artem Korenev, Punit Singh Koura, Marie-Anne Lachaux, Thibaut Lavril, Jenya Lee, Diana Liskovich, Yinghai Lu, Yuning Mao, Xavier Martinet, Todor Mihaylov, Pushkar Mishra, Igor Molybog, Yixin Nie, Andrew Poulton, Jeremy Reizenstein, Rashi Rungta, Kalyan Saladi, Alan Schelten, Silva Ruan, Smith Eric Michael, Subramanian Ranjan, Tan Xiaoqing Ellen, Tang Binh, Taylor Ross, Williams Adina, Xiang Jian, Xu Kuan Puxin, Yan Zheng, Zarov Iliyan, Zhang Yuchen, Fan Angela, Kambadur Melanie, Narang Sharan, Rodriguez Aurelien, Stojnic Robert, Edunov Sergey, and Scialom Thomas. 2023. Llama 2: Open Foundation and Fine-Tuned Chat Models. *arXiv preprint arXiv:2310.12345* (2023).
- [48] Kenneth E Train. 2009. *Discrete choice methods with simulation*. Cambridge university press.
- [49] Amanda L Traud, Peter J Mucha, and Mason A Porter. 2012. Social structure of facebook networks. *Physica A: Statistical Mechanics and its Applications* 391, 16 (2012), 4165–4180.
- [50] Veniamin Veselovsky, Manoel Horta Ribeiro, and Robert West. 2023. Artificial Artificial Artificial Intelligence: Crowd Workers Widely Use Large Language Models for Text Production Tasks. *arXiv:2306.07899* [cs.CL]
- [51] Jesse Vig, Sebastian Gehrmann, Yonatan Belinkov, Sharon Qian, Daniel Nevo, Yaron Singer, and Stuart Shieber. 2020. Investigating gender bias in language models using causal mediation analysis. *Advances in neural information processing systems* 33 (2020), 12388–12401.
- [52] Duncan J Watts and Steven H Strogatz. 1998. Collective dynamics of 'small-world' networks. *nature* 393, 6684 (1998), 440–442.
- [53] Jason Wei, Xuezhi Wang, Dale Schuurmans, Maarten Bosma, Ed Chi, Quoc Le, and Denny Zhou. 2022. Chain of thought prompting elicits reasoning in large language models. *arXiv preprint arXiv:2201.11903* (2022).
- [54] Yuan Yuan, Ahmad Alabdulkareem, and Alex Pentland. 2018. An interpretable approach for social network formation among heterogeneous agents. *Nature communications* 9, 1 (2018), 4704.
- [55] Xuhui Zhou, Hao Zhu, Leena Mathur, Ruohong Zhang, Haofei Yu, Zhengyang Qi, Louis-Philippe Morency, Yonatan Bisk, Daniel Fried, Graham Neubig, et al. 2023. Sotopia: Interactive evaluation for social intelligence in language agents. *arXiv preprint arXiv:2310.11667* (2023).

A FULL REGRESSION TABLE FOR GPT-4 (GPT-4-1106-PREVIEW) AND THE FACEBOOK100 DATA

In Table S.2, we report the regression coefficient for the regression in the real-world network data for all temperatures and GPT-4 (gpt-4-1106-preview). The first column corresponds to the temperature, the next three columns correspond to the fitted coefficients from the regression model of Section 1.C (also shown in Figure 5) accompanied by the standard errors (in parentheses) and the P -values indicated by stars (the null hypothesis corresponds to the parameters being set to 0). Next, LL corresponds to the log-likelihood of the fitted model, and AIC corresponds to the Akaike Information Criterion. Finally, we report the percent change in the accuracy compared to random guessing, the percent change in the average path length (as a measure of the small-world phenomenon), and the clustering coefficient (as a measure of the small-world phenomenon and the triadic closure), as well as the t -statistic for the change in modularity (Q) between the ground truth network dataset (before the edge deletions) and the network after the network formation process.

We observe that $\hat{\theta}_H > \hat{\theta}_{TC} > \hat{\theta}_{PA} > 0$ across all settings. LLM agents do better than random guessing, reinforce the small-world phenomenon, and weaken the triadic closure. Finally, the community structure is strengthened after new links are formed.

Temp.	$\hat{\theta}_{PA}$	$\hat{\theta}_H$	$\hat{\theta}_{TC}$	LL	AIC	% Change Acc.	% Change L	% Change C	ΔQ (t-stat)
Caltech36 (769 nodes, 33,312 edges)									
0.5	0.41*** (0.01)	1.95*** (0.02)	0.59*** (0.01)	-1,377.47	2,762.94	171.8	-0.008	-9.94	3.45**
1.0	0.36*** (0.005)	1.85*** (0.02)	0.58*** (0.01)	-1,435.07	2,878.13	179.6	-0.18	-11.08	3.49**
1.5	0.36*** (0.006)	1.72*** (0.01)	0.55*** (0.007)	-1,522.47	3,052.94	127.6	-0.06	-11.46	3.37**
Swarthmore42 (1,659 nodes, 12,2100 edges)									
0.5	0.18*** (0.003)	1.62*** (0.006)	0.65*** (0.002)	-2,838.33	5,684.66	124.2	0.01	-11.46	7.42***
11.0	0.26*** (0.002)	1.70*** (0.008)	0.58*** (0.003)	-2,927.99	5,863.97	91.6	-0.10	-4.25	1.96*
1.5	0.19*** (0.004)	1.50*** (0.008)	0.59*** (0.002)	-3,139.42	6,286.83	87.39	-0.20	-4.52	4.03***
UChicago30 (6,591 nodes, 416,206 edges)									
0.5	0.23*** (0.001)	2.00*** (0.005)	0.41*** (0.002)	-3,444.33	6,896.67	217.2	-0.24	-2.52	7.46*** [0.34]
1.0	0.23*** (0.002)	1.98*** (0.004)	0.38*** (0.001)	-3,578.18	7,164.36	219.2	-0.12	-2.66	9.56*** [1.05]
1.5	0.22*** (0.004)	1.78*** (0.008)	0.41*** (0.002)	-2,033.49	4,074.98	222.4	-0.17	-2.42	10.19*** [0.24]
<p>Notes $\hat{\theta}_{PA}$ = Coefficient of log degree, $\hat{\theta}_H$ = Coefficient of log # of common attributes, $\hat{\theta}_{TC}$ = Coefficient of log # common neighbors LL = Log-likelihood, AIC = Akaike Information Criterion Acc. = Accuracy, L = Average Path Length, C = Average Clustering Coefficient, ΔQ (t-stat) = Modularity change t-statistic * : $P < 0.05$, ** : $P < 0.01$, *** : $P < 0.001$</p>									

Table S.2. Multinomial logit coefficients for three networks from the Facebook100 dataset and GPT-4 (gpt-4-1106-preview). The standard errors of the estimates are shown in parentheses. The null hypothesis corresponds to the respective parameter being equal to 0. We report the percent change in accuracy, average path length, and average clustering coefficient compared to the initial network (before the deletion of edges). For the change in modularity, we run the Louvain algorithm ten times and perform a t-test with the resulting modularities. For the UChicago30 dataset, we report the t-statistic value in the subgraph induced by the 2,000 sampled nodes, since the newly added edges would have a very small effect on the change in the community structure if we were to measure it in the whole network. We also report the modularity change (t-statistic) of the whole graph inside brackets.

A.1 Analytical Regression Tables for GPT-4 (gpt-4-1106-preview)

We present the regression tables for all the combinations of coefficients for each of the three real-world network datasets. For all datasets, we observe that $\hat{\theta}_{PA}$ is smaller than both $\hat{\theta}_{TC}$ and $\hat{\theta}_H$ in all models where any pair is included. Similarly, $\hat{\theta}_{TC}$ is always smaller than $\hat{\theta}_H$ in all models that

are both included. Finally, note that whenever only $\hat{\theta}_{PA}$ and $\hat{\theta}_{TC}$ are considered, then $\hat{\theta}_{PA} < 0$ and the result is not statistically significant ($P > 0.05$).

Temp.	$\hat{\theta}_{PA}$	$\hat{\theta}_H$	$\hat{\theta}_{TC}$	Log Likelihood	AIC
0.5	0.50*** (0.001)			-2,236.36	4,476.71
0.5		2.78*** (0.003)		-1,511.42	3,026.85
0.5			1.53*** (0.002)	-1,506.01	3,016.02
0.5	0.64*** (0.002)	2.99*** (0.007)		-1,414.71	2,835.41
0.5	-0.02 (0.003)		1.53*** (0.003)	-1,505.95	3,017.90
0.5		1.43*** (0.004)	0.82*** (0.002)	-1,406.39	2,818.78
0.5	0.41*** (0.01)	1.95*** (0.02)	0.59*** (0.01)	-1,377.47	2,762.94
1.0	0.48*** (0.001)			-2,242.85	4,489.70
1.0		2.69*** (0.003)		-1,558.67	3,121.34
1.0			1.47*** (0.002)	-1,556.68	3,117.37
1.0	0.58*** (0.002)	2.86*** (0.003)		-1,473.13	2,952.26
1.0	-0.04 (0.002)		1.47*** (0.002)	-1,556.24	3,118.48
1.0		1.40*** (0.01)	0.79*** (0.002)	-1,457.76	2,921.52
1.0	0.36*** (0.005)	1.85*** (0.02)	0.58*** (0.01)	-1,435.07	2,878.13
1.5	0.50*** (0.001)			-2,233.25	4,470.50
1.5		2.51*** (0.003)		-1,646.83	3,297.65
1.5			1.36*** (0.001)	-1,636.20	3,276.40
1.5	0.57*** (0.002)	2.65*** (0.005)		-1,559.57	3,125.15
1.5	-0.01 (0.002)		1.37*** (0.002)	-1,636.19	3,278.37
1.5		1.29*** (0.004)	0.75*** (0.002)	-1,546.78	3,099.55
1.5	0.36*** (0.006)	1.72*** (0.01)	0.55*** (0.007)	-1,522.47	3,052.94

Note

* : $P < 0.05$, ** : $P < 0.01$, *** : $P < 0.001$

Table S.3. Multinomial logit coefficients for Caltech36 and GPT-4 (gpt-4-1106-preview). The standard errors of the estimates are shown in parentheses.

Temp.	$\hat{\theta}_{PA}$	$\hat{\theta}_H$	$\hat{\theta}_{TC}$	Log Likelihood	AIC
0.5	0.33*** (0.0007)			-4,978.28	9,960.56
0.5		2.91*** (0.001)		-3,027.03	6,058.06
0.5			1.37*** (0.0006)	-3,014.28	6,032.57
0.5	0.44*** (0.004)	2.99*** (0.003)		-2,948.91	5,903.82
0.5	-0.18*** (0.002)		1.36*** (0.002)	-3,002.17	6,010.35
0.5		1.42*** (0.003)	0.72*** (0.002)	-2,847.16	5,700.32
0.5	0.18*** (0.003)	1.62*** (0.006)	0.65*** (0.002)	-2,838.33	5,684.66
1.0	0.38*** (0.0007)			-4,959.02	9,922.04
1.0		2.83*** (0.001)		-3,119.06	6,242.11
1.0			1.32*** (0.0006)	-3,118.13	6,240.26
1.0	0.50*** (0.004)	2.92*** (0.002)		-3,018.85	6,043.71
1.0	-0.11** (0.002)		1.32*** (0.002)	-3,113.21	6,232.43
1.0		1.41*** (0.004)	0.69*** (0.003)	-2,947.89	5,901.78
1.0	0.26*** (0.002)	1.70*** (0.008)	0.58*** (0.003)	-2,927.99	5,863.97
1.5	0.36*** (0.0007)			-4,952.51	9,909.02
1.5		2.64*** (0.001)		-3,324.71	6,653.43
1.5			1.24*** (0.0006)	-3,306.06	6,616.11
1.5	0.44*** (0.003)	2.71*** (0.001)		-3,241.67	6,489.35
1.5	-0.14*** (0.003)		1.24*** (0.001)	-3,298.07	6,602.13
1.5		1.30*** (0.003)	0.67*** (0.002)	-3,150.29	6,306.57
1.5	0.19*** (0.004)	1.50*** (0.008)	0.59*** (0.002)	-3,139.42	6,286.83

Note

* : $P < 0.05$, ** : $P < 0.01$, *** : $P < 0.001$

Table S.4. Multinomial logit coefficients for Swarthmore42 and GPT-4 (gpt-4-1106-preview). The standard errors of the estimates are shown in parentheses.

Temp.	$\hat{\theta}_{PA}$	$\hat{\theta}_H$	$\hat{\theta}_{TC}$	Log Likelihood	AIC
0.5	0.28*** (0.02)			-5,983.56	11,971.13
0.5		2.93*** (0.05)		-3,637.18	7,278.37
0.5			1.11*** (0.02)	-3,740.78	7,485.55
0.5	0.38*** (0.04)	3.06*** (0.21)		-3,523.06	7,052.12
0.5	-0.04 (0.08)		1.11*** (0.04)	-3,739.31	7,484.61
0.5		1.68*** (0.13)	0.51*** (0.07)	-3,477.37	6,960.75
0.5	0.23*** (0.06)	2.00*** (0.24)	0.41*** (0.09)	-3,444.33	6,896.67
1.0	0.28*** (0.02)			-5,982.66	11,969.32
1.0		2.85*** (0.05)		-3,759.78	7,523.56
1.0			1.07*** (0.02)	-3,879.04	7,762.08
1.0	0.36*** (0.07)	2.96*** (0.31)		-3,649.84	7,305.68
1.0	-0.04 (0.06)		1.07*** (0.03)	-3,877.83	7,761.66
1.0		1.67*** (0.11)	0.49*** (0.08)	-3,611.48	7,228.95
1.0	0.23*** (0.10)	1.98*** (0.17)	0.38*** (0.06)	-3,578.18	7,164.36
1.5	0.30*** (0.03)			-3,241.67	6,487.34
1.5		2.71*** (0.06)		-2,145.02	4,294.03
1.5			1.03*** (0.02)	-2,175.32	4,354.64
1.5	0.37*** (0.08)	2.81*** (0.10)		-2,080.67	4,167.34
1.5	-0.01 (0.04)		1.03*** (0.04)	-2,175.25	4,356.49
1.5		1.50*** (0.10)	0.51*** (0.04)	-2,051.61	4,109.23
1.5	0.22*** (0.12)	1.78*** (0.27)	0.41*** (0.07)	-2,033.49	4,074.98

Note

* : $P < 0.05$, ** : $P < 0.01$, *** : $P < 0.001$

Table S.5. Multinomial logit coefficients for UChicago30 and GPT-4 (gpt-4-1106-preview). The standard errors of the estimates are shown in parentheses.

B NETWORK EVOLUTION AND OMITTED SIMULATIONS

Here we depict the evolution of the networks generated by the LLM agents, as well as omitted simulations.

B.1 Principle 1: Preferential Attachment

Network Evolution. We plot the evolution of the LLM-based preferential attachment networks at three timesteps, together with the degree distribution alongside the degree distribution of a BA graph with the same number of nodes. We observe that for the temperature being 0.5 we have a core-periphery-like formation which diverges from the BA model, whereas for the temperature being 1.5 the network has the same degree distribution as the BA model.

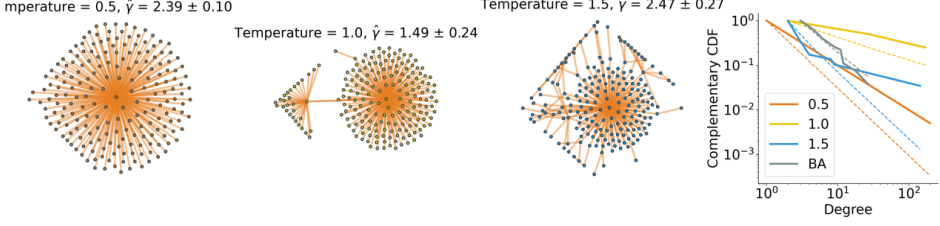


Fig. S.9. Results for Principle 1 (preferential attachment): We display simulated networks comprising 200 nodes across different temperatures. For the degree-based simulations, node degree data $\{d_{j,t} : j \in V_t\}$ was provided (V_t corresponds to the vertex set of the network G_t at round t). With degree information only, the networks form more unrealistic star-like structures, diverging from scale-free configurations and more closely mirroring a core-periphery network structure.

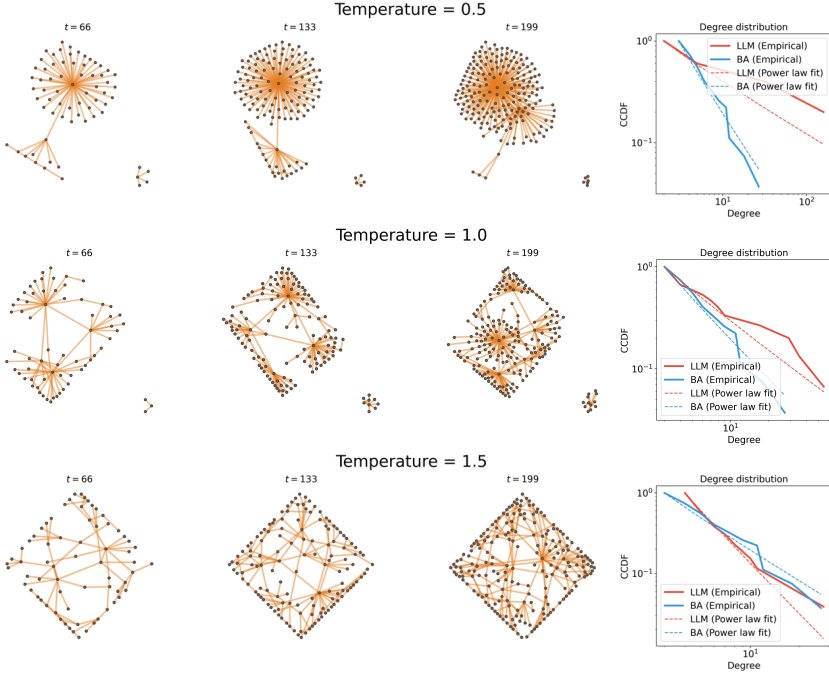


Fig. S.8. Dynamic evolution of networks created based on Principle 1.

Simulations with Degree Information. In Figure S.9 we provide the results with degree-information only. We observe that the agents form connections around high-degree nodes only (see Figure S.9). The same result (star-like networks) holds for the other LLM models and temperatures.

B.2 Principle 2: Triadic Closure

Network Evolution. We plot the evolution of the LLM-generated networks based on the triadic closure principle, together with the transitivity measure and the algebraic connectivity (which corresponds to the second-smallest eigenvalue of the graph Laplacian). We observe that the algebraic connectivity gradually increases as new edges between the clusters are created. Specifically, the

algebraic connectivity reaches a higher value for higher temperatures, indicating the more frequent creation of new intra-cluster edges. Moreover, we observe that the transitivity initially increases and then decreases until it reaches its final value.

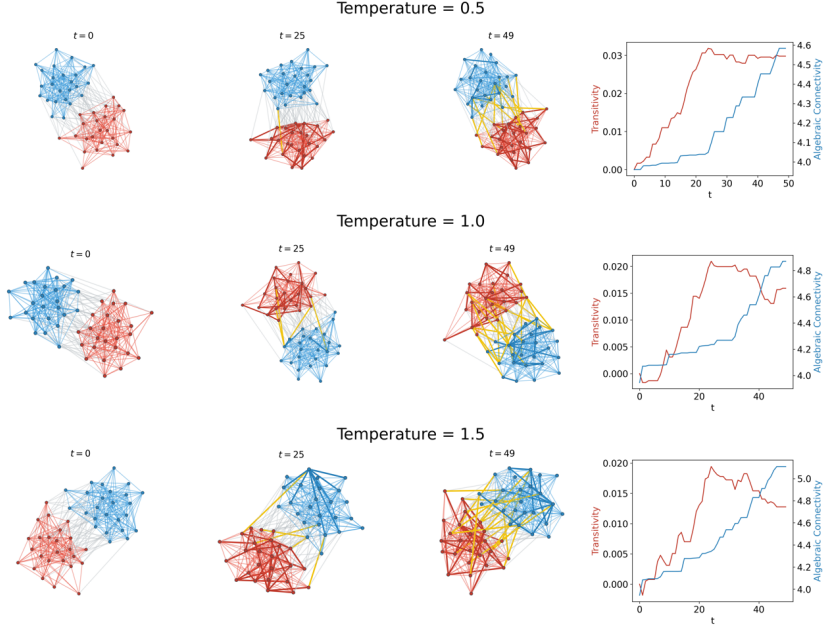


Fig. S.10. Dynamic evolution of networks created based on Principle 2.

Simulations with the Number of Common Neighbors. Instead of giving the neighborhood information, the simulations presented in Figure S.11 use the number of common neighbors. We observe behavior similar to Figure 2.

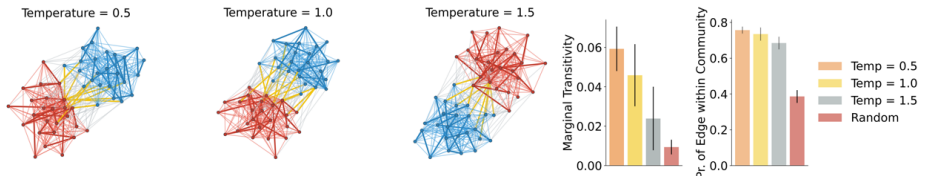


Fig. S.11. **Results for Principle 2 (triadic closure).** The figure shows the same networks as in Figure 2 with the only change that instead of the intersection of neighborhoods between the query node and each alternative, we provide the number of common neighbors (i.e., the size of the intersection) between the query node and each alternative. Similarly, we observe that the probability of forming an edge within the same community and the marginal transitivity, which indicate triadic closure, is significantly larger than randomly creating links ($P < 0.001$, t-test). The error bars correspond to 95% confidence intervals.

ALGORITHM 3: Example prompt regarding social network data with Chain-of-Thought reasoning. Note that compared to Algorithm 1 the order of the fields name and reason in the output format is reversed.

```

# Task
You are located in a school. Your task is to select a set of people to be friends with.

# Profile
Your profile is given below after chevrons:
<PROFILE>
{
    "name" : "Person 0",
    "favorite subject" : "Chemistry",
    "neighbors" : ["Person 3", "Person 432", "Person 4", "Person 3", "Person 32"]
}
</PROFILE>

# Candidate Profiles
The candidate profiles to be friends with are given below after chevrons:

<PROFILES>
[
    {
        "name" : "Person 1",
        "favorite subject" : "Mathematics",
        "neighbors" : ["Person 3", "Person 4", "Person 23", "Person 65"]
    },
    {
        "name" : "Person 33",
        "favorite subject" : "History",
        "neighbors" : ["Person 342", "Person 2", "Person 12"]
    },
    ...
]
</PROFILES>

# Output
The output should be given a list of JSON objects with the following structure

[
    {
        "reason" : reason for selecting the person,
        "name" : name of the person you selected
    },
    ...
]

# Notes
- The output must be a list of JSON objects ranked in the order of preference.
- You can make at most 1 selection.

```

C CHAIN-OF-THOUGHT EXPERIMENTS

We experiment with Chain-of-Thought (CoT) reasoning [53]. To induce CoT reasoning we ask the LLM agents to output the reason and then their choice (i.e. by reversing the order of reason and name in Algorithm 2). The resulting prompt can be found at Algorithm 3. In the following figures, we show the results from the same experiments as the ones we of the main text with the different that CoT is used.

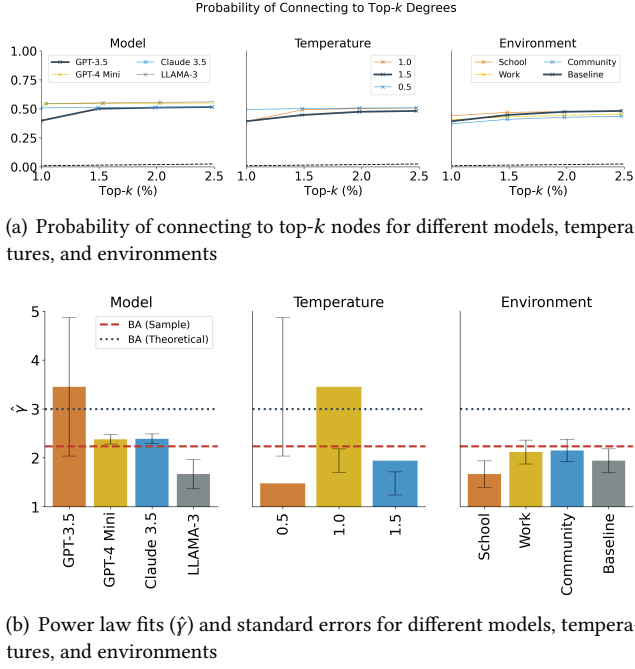


Fig. S.12. **Results for Principle 1 with CoT reasoning (preferential attachment)** The multi-LLM setup was given neighborhood information $\{N_{j,t} : j \in V_t\}$. **Top:** Probability of connecting to top- k -degree nodes for varying model (temperature is fixed to 1.0 and environment to baseline), temperature (model fixed to GPT-3.5 and environment to baseline) and environment (model fixed to GPT-3.5 and environment temperature to 1.5) for networks generated according to Principle 1 with $n = 200$ nodes. **Bottom:** Power Law exponents and standard errors for varying model, temperature, and environment.

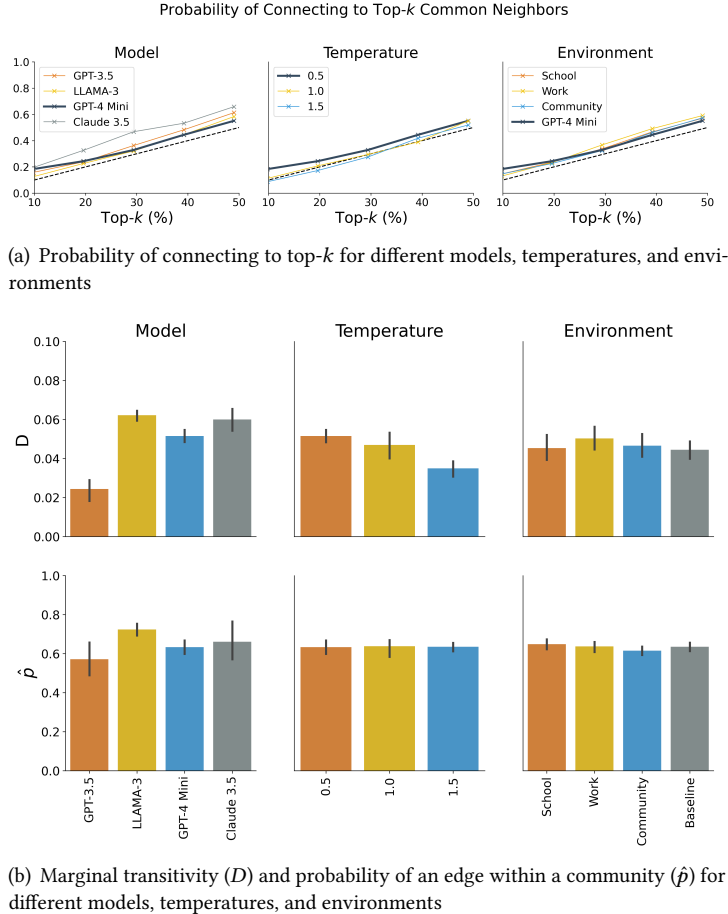
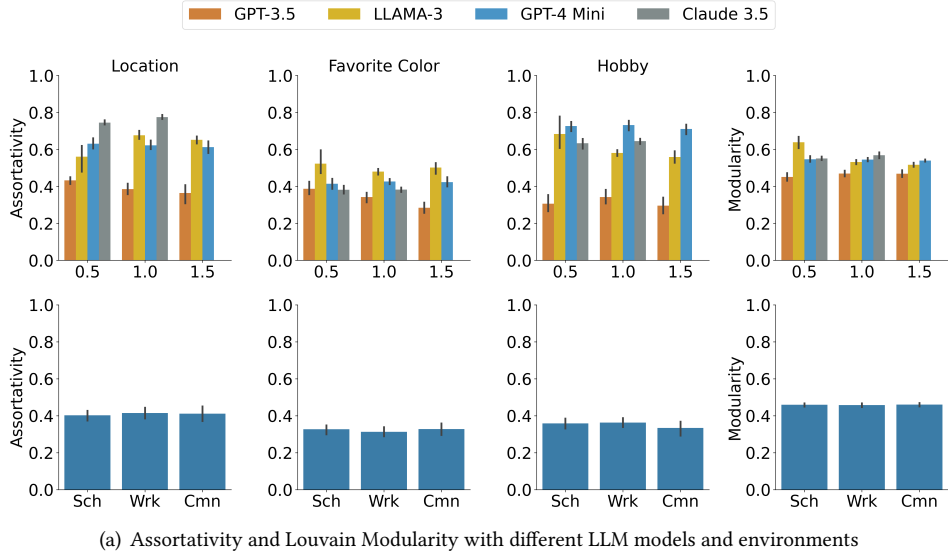


Fig. S.13. **Results for Principle 2 with CoT reasoning (triadic closure).** **Top:** Probability of connecting to top- k nodes (in terms of common neighbors) for varying model (temperature is fixed to 1.0 and environment to baseline), temperature (model fixed to GPT-4 Mini and environment to baseline) and environment (model fixed to GPT-4 Mini and environment temperature to 0.5) for networks generated according to Principle 2 ($n = 50$, 10 simulations for each model, environment and temperature). **Bottom:** Marginal transitivity (D) and probability of an edge within a community (\hat{p}) for networks generated according to Principle 2 in different models, temperatures, and environments.



(a) Assortativity and Louvain Modularity with different LLM models and environments

Fig. S.14. **Results for Principle 3 (Homophily) and Principle 4 (Community structure due to homophily) with CoT reasoning.** Top: Assortativities and Louvain modularity according to Principle 3 ($n = 50$, 5 simulations for each row) in different environments (school, work, community) using different models. The statistical significance is $P < 0.001$ for all t-tests (comparing with 0).

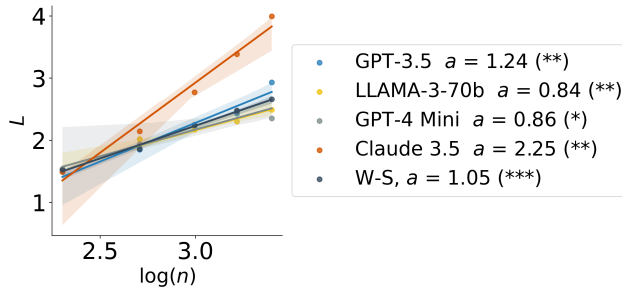
(a) Regression plot for different models and environments for $\beta = 0.25$ and $k = 5$.

Fig. S.15. **Fitted results for Principle 5 with CoT reasoning (small world).** Regression plot for the relation $L \sim \log(n)$ for different LLM models for $\beta = 0.25$ and $k = 5$. The legend shows the effect size (a) and the P -value. (*: $P < 0.05$; **: $P < 0.01$, and ***: $P < 0.001$.)